DESIGN AND INSTALLATION

OF A HIGH REYNOLDS NUMBER

RECIRUCLATING WATER TUNNEL

By

LIBIN DANIEL

Bachelor of Science in Aerospace Engineering

Embry-Riddle Aeronautical University

Prescott, AZ

2012

Submitted to the Faculty of the
Graduate College of the
Oklahoma State University
in partial fulfillment of
the requirements for
the Degree of
MASTER OF SCIENCE
July, 2014

ProQuest LLC.
789 East Eisenhower Parkway
P.O. Box 1346
Ann Arbor, MI 48106 - 1346

DESIGN AND INSTALLATION

OF A HIGH REYNOLDS NUMBER

RECIRUCLATING WATER TUNNEL

Thesis Approved:

Dr. Brian Elbing

Thesis Adviser

Dr. Jamey Jacob

Dr. Arvind Santhanakrishnan

ACKNOWLEDGEMENTS

I dedicate this work and this education to my parents who are the epitome of self-sacrifice and trust. They have assured that I had every possible resource I needed to accomplish my goals and fulfill my dreams, and they trusted in me more than I did in myself, throughout this journey. Thank you for everything.

This project would not have achieved so much in such a short time without the constant advice, guidance and assistance from my research advisor, Dr. Elbing. Thank you so much for being continually patient with me and providing me with all the resources and knowledge needed to accomplish these goals. I would also like to thank Dr. Arena for his initial guidance in regards to composites fabrication.

I would also like to acknowledge the help and assistance provided by the vendors we have utilized for this project. I would like to thank JR Purvis from ePumps for his constant willingness to help and go that extra mile. I would also like to thank Dan Diehl and Kyle McCreary for their fabrication efforts. I would also like to thank Weamcometric Industrials for their support.

My stay at Stillwater would not have been this enjoyable without my friends at the Newman center here at Oklahoma State University. Thank you so much for your love, fellowship, wisdom and the bucket loads of fun we had during my stay here. Life would have been quite dull without it. I would also like to thank my dearest friend, Jake, for continually believing in me and pushing me to do the best I possibly can. I am so glad that God placed you in my life.

Finally, I would like to thank the Lord and the communion of saints for giving me enough wisdom and knowledge to finish this project in a timely matter. Looking back, I have numerous moments when I was guided not just by my own skills and knowledge. I hope this work brings glory to His name and is in accord to His will for me. I would also like to acknowledge the intercession of St. Albert the Great, St. Thomas Aquinas and St. Augustine in helping me with the completion of this thesis in such a short time, and St. Anthony for helping me to not loose my mind!

Acknowledgements reflect the views of the author and are not endorsed by committee members or Oklahoma State University.

Name: LIBIN DANIEL

Date of Degree: JULY, 2014

Title of Study: DESIGN AND INSTALLATION OF A HIGH REYNOLDS NUMBER RECIRUCLATING WATER TUNNEL

Major Field: MECHANICAL AND AEROSPACE ENGINEERING

Abstract: The High-Reynolds Number Fluid Mechanics Laboratory has recently been established at Oklahoma State University (OSU). The three primary components of the laboratory are 1) a recirculating water tunnel, 2) a multiphase pipe flow facility, and 3) a multi-scale flow visualization system. This thesis focuses on the design and fabrication of the water tunnel, which will be used for high-Reynolds number turbulent boundary layer research.

Two main design criteria for the water tunnel were to achieve a momentum thickness based Reynolds number in excess of 10^4 and to have high optical access to the flow surfaces in the test section. This is being achieved with a 1 m. long test section and a maximum flow speed of 10 m/s. This Reynolds number was targeted to bridge the gap between typical university water tunnels (10^3) and the world's largest water tunnel facilities (10^5). The water tunnel is powered by a 150 hp motor and a 4500 gpm capacity centrifugal pump. The water tunnel is designed for a maximum operating pressure of 40 psi. This will make the facility a low cost option to perform high-Reynolds number aerodynamic and hydrodynamic tests. Improved flow imaging capability is a major advantage to liquid based fluid facilities because of the increased density for seeding and reduced field-of-view for equivalent Reynolds number. The laboratory's state-of-the-art flow visualization system can be used for time-resolved and phase averaged stereo-particle-image-velocimetry (sPIV), laser-induced-fluorescence, and high-speed imaging. Design provisions are also made to allow a multi-phase loop to share the pump and motor configuration of this water tunnel facility.

The major design decisions that went into the design of the water tunnel facility are discussed. The design considerations that were taken into account for the test section, flow conditioning sections and the entire flow loop are discussed in greater detail. The final configuration and the technical drawings of the water tunnel flow loop, the test section, the contraction and diffuser sections are also provided. The installation procedure that will be utilized to install the water tunnel in the High Reynolds Number Fluid Mechanics Laboratory is also discussed.

TABLE OF CONTENTS

LIST OF TABLES

LIST OF FIGURES

CHAPTER I

INTRODUCTION

1.1 Motivation

A new high-Reynolds number experimental fluid mechanics laboratory has recently been established at Oklahoma State University (OSU) that will expand upon OSU's existing aerodynamics and fluid dynamics capabilities and expertise. The primary facility of this new laboratory will be a high-Reynolds number recirculating water tunnel, which will compliment OSU's high-Reynolds number, subsonic wind tunnel. Additional features of the new laboratory include a multiphase pipe flow loop that will use the water tunnel's pump and a multi-scale flow visualization system. The water tunnel design and integration with these additional laboratory capabilities is the focus of this thesis.

While the OSU subsonic wind tunnel can achieve Reynolds numbers comparable to the water tunnel being designed, the new facility is being built for improved flow visualization as well as to study Naval drag reduction applications. The new laboratory's multi-scale flow visualization system can be better utilized in water because of the higher density (1000 times denser than air) and lower kinematic viscosity (15 times less than air at room temperature). Flow diagnostic tools that involve imaging, like particle image velocimetry (PIV), require the addition of flow tracers that must be large enough to image while small enough to accurately follow the flow. The much larger density of water allows for relatively large particles to accurately follow

the flow-field, which reduces the signal-to-noise ratio and ultimately increases the measurement accuracy. The lower kinematic viscosity enables higher Reynolds number flow to be achieved over physically smaller models. These smaller sizes require less laser power and small optical components, which significantly reduces the cost and complexity required to image a given flow-field.

The water tunnel is also a requirement in order to study drag reduction technologies for the US Navy. In recent years, the US Navy has focused on four drag reduction technologies for surface and subsurface vehicles: polymer additives, air layers, partial cavities, and superhydrophobic surfaces. All these technologies involve the addition of air or polymers into a high-Reynolds number turbulent boundary layer. The polymer additives must remain hydrated in order for the drag reduction mechanism to be active, which requires a liquid boundary layer. Moreover, the other drag reduction techniques utilize the significantly reduced density of air to reduce the drag. Thus to properly capture the physics in a wind tunnel, a gas that is a 1000 times lighter than air would have to be used as the boundary layer additive.

Thus, the current work aims to design a high-Reynolds number water tunnel with maximum optical access while remaining rigid, which can be used for future Naval drag reduction studies.

1.2 Review of Primary Components of a Water Tunnel

Water tunnels are utilized to experimentally perform fluid dynamics research using either the boundary layer that forms on the walls or model studies aimed at characterizing or improving aerodynamic or hydrodynamic characteristics of a vehicle. While the design of a water tunnel is

driven by its specific design objectives, the main components (illustrated in Figure 1) of any water tunnel are the same.

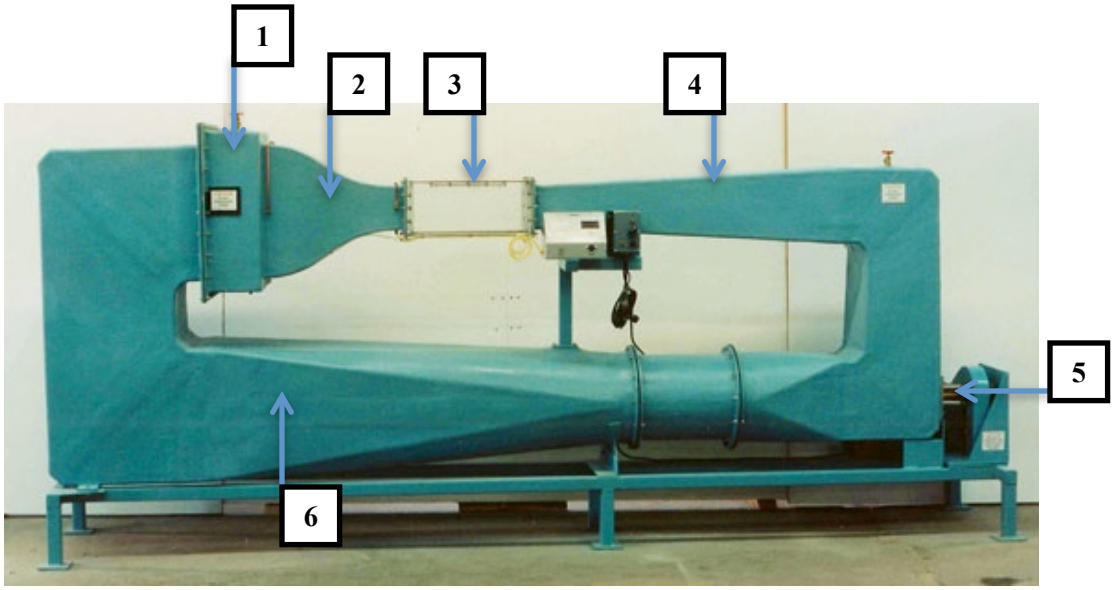

Figure 1: Image of a typical commercially available water tunnel

Source: (http://www.aerolab.com/img/Water_Tunnel/img/4.jpg).

A typical water tunnel (6×6 Closed Circuit Water Tunnel, Aerolab) is shown in Figure 1 with the primary components numbered: (1) flow conditioning, (2) contraction, (3) test section, (4) diffuser, (5) pump and (6) return leg piping. The individual components are described below:

(1) Flow Conditioning Unit

The purpose of the flow-conditioning section is to suppress free-stream turbulence and straighten out the flow (i.e. remove any swirl in the flow). It is generally comprised of some combination of honeycomb sections, screens and settling chambers. The sizing is dependent on the acceptable turbulence level in the test section free-stream, available pressure drop (based on pump sizing, operating speed and other system losses), and resource limitations (economic and space constraints). A detailed honeycomb design routine is described in Lumley and McMahon

(1967). The typical configuration has the honeycomb section placed upstream of the test section and contraction, separated by a settling chamber section. The honeycomb straightens the flow, and the settling chamber length is designed to allow turbulence from the honeycomb to decay. Wetzel and Arndt (1994) provide theoretical estimates and experimental results on the expected turbulence levels in the test section with the addition of a honeycomb.

(2) Contraction

The purpose of the contraction section is to accelerate the flow and to reduce turbulence levels in the test section. Desired turbulence levels, resource limitations (economic and space constraints) and manufacturability define the area ratio of the contraction. The length of the contraction ratio is based on space constraints and to assure turbulence suppression. The contraction section is generally placed right before the test section. The contraction profile is commonly fit to a fifth-order polynomial as described in Bell and Mehta (1988). Ripken (1951) states that conventional water tunnels have contraction ratios between six and nine.

(3) Test Section

The purpose of the test section is to create a platform for conducting experiments. The design of the test section is impacted by the desired flow quality of the flow stream, the operational range and instrumentation constraints. The mating requirements with other components adjacent to the test section, i.e. contraction and diffuser sections, also impact the design of the test section. For a flat plate boundary layer research facility, the test surface sizing is based on flat plate theory as detailed by White (White 2006). A water tunnel designed for model studies generally utilizes a rectangular or circular cross section. The target Reynolds number defines the size of the test section and the desired test speed.

(4) Diffuser

The purpose of the diffuser section is to slow down the flow and to regain pressure. The diffuser section is generally located immediately downstream of the test section. The fast flowing water stream is decelerated by diffusing the flow via an increase in cross sectional area. The diffuser angle is typically selected based on the space available for the water tunnel facility and the maximum area expansion angle without causing flow separation. Experimental results by Nikuradse are highlighted in one of the design studies of the St. Anthony Falls water tunnel facilities (Purdy and Straub 1948). Nikuradse showed that non-symmetrical velocity distributions start occurring in an expanding rectangular conduit when the half angle is 4°. The simulation results of the diffuser section at UNH (Nedyalkov 2012) also impacted the diffuser section design for this water tunnel facility. The results show that, even at 3.5°, no separation is observed for circular expanding conduits.

(5) Pump and Motor

The pump provides the required pressure differential to drive the water through the tunnel loop. The pump size is based on the test section size, flow speed range and total system losses. These factors are defined by the overall tunnel design objectives, the complete tunnel design and resource availability. The pump type selection is driven by the tunnel objectives and the desired flow characteristics at the test section. For example, a flow loop designed to study medical topics like the blood flow through arteries requires a pulsating flow. This requires a piston pump. However, a research facility designed for investigating non-newtonian fluid flow would require a progressive cavity pump.

A typical water tunnel designed for turbulence research of Newtonian fluids at high speeds desire minimal turbulence level at the test section. An axial pump provides the least

turbulence levels at the outlet flow. However, a centrifugal pump is a more cost effective solution for a given flow capacity. Based on the pump selection and the pressure head loss estimates for the entire flow loop, a power estimate can be obtained. This power estimate drives the selection of the motor size. The pump is generally placed sufficiently away from the test section such that the flow stream can be conditioned using honeycombs and screens and sped up through a contraction section before the flow reaches the test section.

(6) Return leg piping

The sizing and design of the return leg is driven by integration requirements with other components, drain locations, avoidance of flow separation and resource availability. Resource availability and the minimum half angle to avoid flow separation define the length of the piping sections and the cone angle. Integration with the existing components defines the diameter of the piping sections. The drain location and instrumentation requirements lead to the drain hole and pressure port locations.

1.3 Review of Existing Water Tunnels

The water tunnel design, described in this thesis, draws upon the knowledge established during the design and operation of other high-speed water tunnels. Table 1 provides a review of these key facilities and the available literature used as a reference for the design of the current water tunnel facility. Table 1 lists some of the most prominent water tunnel facilities in the world. It can be noted that the LCC has the largest test section. The mini LCC water tunnel at University of Michigan (USA) has the highest test section speed. It can be noted that the water tunnel at Oklahoma State University is comparable in size and capability to other small water tunnels like the HiCaT at University of New Hampshire (Nedyalkov, 2012).

Table 1: List of prominent water tunnels

Name	Ownership	Test Section Dimensions (in.)	Max. Speed (m/s)	Associated Literature
Large Cavitation Channel (LCC)	NAVSEA, Carderock (USA)	120 x120	18	Etter *et al.*, 2005
HYKAT	HSVA (Germany)	110 x 63	12	Arndt and Weitendorf, 1990
LOCAT	MOERI (Korea)	110 x 70	15	Wosnik and Arndt, 2006
St. Anthony Falls High-Speed Water Tunnel	University of Minnesota (USA)	7.4 x 7.4	20	Arndt et al. (1991)
Mini-LCC	University of Michigan (USA)	8.6 x 8.6	25	Shen et al. (2006); Makiharju et al. (2013)
High-Speed Cavitation Tunnel (HiCaT)	University of New Hampshire (USA)	6 x 6	17	Nedyalkov, 2012
Tunnel de Cavitation	Ecole Navale (France)	7.6 x 7.6	15	Leroux et al. (2004)
Grand Tunnel Hydrodynamique (GTH)	Bassin d'Essais des Carènes (France)	44.9 x 44.9	20	Gindroz & Billet (1998)
Flow Noise Simulator (FNS)	Naval Systems Research Center (Japan)	91.7 x 91.7	15	Mori et al. (2003)
9-inch Water Tunnel	University of Michigan (USA)	9 (diameter)	18	Oweis et al. (2004)
Garfield Thomas Water Tunnel	Pennsylvania State University (USA)	48 (diameter)	18	Lehman (1959); Lauchle & Gurney (1984)
12-inch Water Tunnel	Pennsylvania State University (USA)	12 (diameter)	24	Madavan *et al.* (1984); Deutsch & Castano (1986); Fontaine & Deutsch (1992)
6-inch Water Tunnel	Oklahoma State University (USA)	6 x 6	12	Current Thesis

1.4 OSU Facilities

OSU currently has the following wind and water facilities that are geared towards fluids and aerodynamics research:

1. Small undergraduate wind tunnel
2. Large subsonic wind tunnel
3. Small open channel undergraduate water tunnel
4. Undergraduate Water Tunnel (in progress)

With this high Reynolds number water tunnel, the OSU facilities will benefit from a low turbulence, high Reynolds number test section that can utilize the flow diagnostic tools available. This water tunnel will focus on drag reduction research involving turbulent boundary layer that are modified using hydrated polymers.

The flow visualization system for the laboratory includes a high-speed diode pumped laser (30 mJ/pulse at 1 kHz), a pair of high resolution (5.5 megapixel) sCMOS cameras, and a pair of high-speed (1.6 kHz at full resolution) CMOS cameras. This system can be used for time-resolved and phase averaged stereo-particle-image-velocimetry, laser-induced-fluorescence, and high-speed imaging measurements

CHAPTER II

OVERALL DESIGN CONSTRAINTS

2.1 Design Objectives

The design objectives for this water tunnel facility are:

- *Obtain a high Reynolds number turbulent boundary layer*

This water tunnel will be mainly utilized for polymer based drag reduction experiments for Naval applications. The focus of these experiments will be to document the drag reduction capabilities at a Reynolds number equivalent to full-scale environment. The boundary layer in a full-scale environment is turbulent in nature. As a result, the test section should be able to provide a high Reynolds number turbulent boundary layer. This requirement would also define the final surface finish requirements for the test surfaces.

- *Maximum optical access within test section to utilize flow visualization capabilities*

High-speed flow visualization, primarily PIV, will be the main diagnostic tool that will be utilized to study the turbulent boundary layer. As a result, the test section will be designed such that the optical equipment has a clear and unobstructed access to the boundary layer that is being imaged.

- *Obtain low turbulence intensity values in the test section*

Lower turbulence intensity values are a measure of a cleaner flow stream. In order to assure that the experiments are controlled, and that random turbulence fluctuations do not affect the results of the experiment, a low turbulence intensity of less than 0.1% is desired in the test section.

- *Maximum operational pressure of 40 psi*

By pressurizing the water tunnel flow loop, cavitation concerns can be negated by increasing the pressure of the flow above the vapor pressure of the water. This will avoid abrupt pressure loss and poor flow quality due to cavitation.This will also avoid damage to the water tunnel since cavitation destroys the flow surface.

2.2 Overall Design

The overall design and layout of this water tunnel is shown in Figure 2. The water tunnel is composed of sixteen (16) primary components, which are listed in the table within Figure 2. The component numbering starts with the first elbow (top left corner) and increases in the flow direction. Specific details about the design routine for each of these components are discussed in the Chapter 3, starting with the test section.

Part Number	Description	Part Number	Description
1	Elbow 1	9	Down Leg Piping
2	Honeycomb (HC1)	10	Elbow 3
3	Settling Chamber and Honeycomb (HC2)	11	10" X 12" Rolled Cone
4	Contraction	12	Pump Inlet Piping
5	Test Section	13	Pump and Motor
6	Diffuser	14	10' X 20" Rolled Cone
7	Straight Pipe	15	Elbow 4
8	Elbow 2	16	Up Leg

Figure 2: Overview of water tunnel flow loop with labeled individual components

2.3 Laboratory (Space/Layout)

The water tunnel will be located in the High-Reynolds Number Fluid Mechanics Laboratory at Oklahoma State University. Thus the space constraints for the water tunnel are that it should be able to fit within this laboratory, which has dimensions of 49.4 ft. (length) × 20.1 ft. (width) × 9 ft. (height). The overall layout of the laboratory, including the water tunnel, is schematically shown in Figure 3.

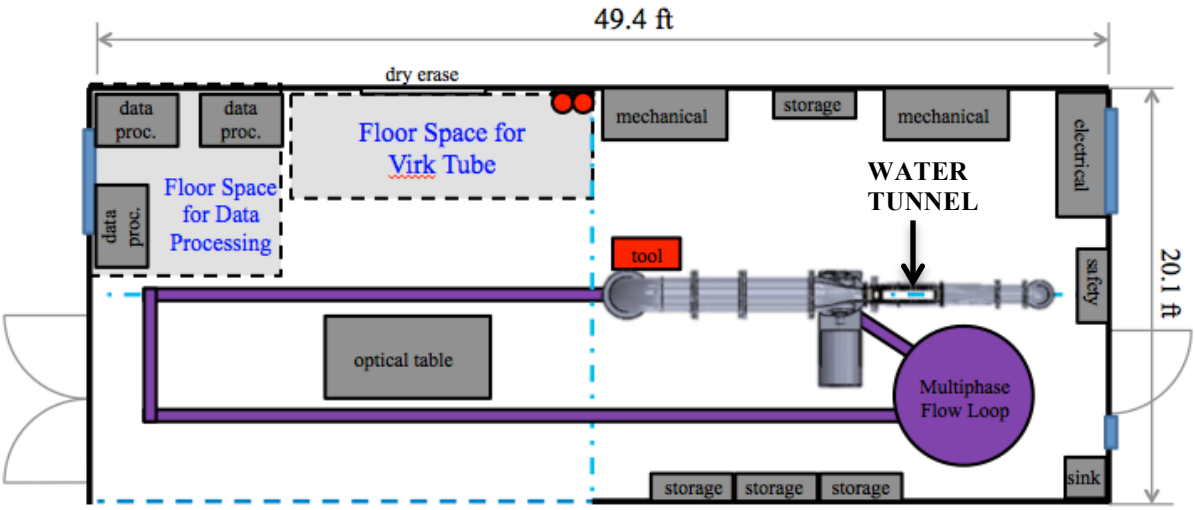

Figure 3: Proposed layout of the available laboratory space (ATRC 150) including the position of the water tunnel.

The positioning of the water tunnel in the laboratory space is shown in Figure 3. The water tunnel shares the laboratory space with PIV data processing computer stations, "Virk Tube" setup used for characterizing polymer solution and the multi-phase flow loop. The position allows easy access to the test section. The water tunnel is located such that the multi-phase flow loop can utilize the pump and motor efficiently. This location was also affected by the location of an I-beam on the ceiling of the room. This I-beam will be used during the assembly process and also for future operations. This water tunnel location would also allow the setting up of laser safety

curtains. These safety curtains would help in not disrupting the work in other parts of the lab while the laser for the PIV system is operational.

CHAPTER III

TEST SECTION DESIGN

The primary purpose of this water tunnel is to study turbulent boundary layers. Boundary layers are strongly influenced by Reynolds number, *Re*, a fundamental non-dimensional parameter used to quantify the balance between inertial and viscous forces,

$$Re = \frac{UL}{\nu}.$$

Equation 1

Here *U* is the characteristic velocity of the given flow, *L* is a characteristic length scale and ν is the kinematic viscosity of the fluid. In turbulent boundary layer research, it is common to use the momentum-thickness (θ) as the characteristic length scale, which results in the momentum-thickness based Reynolds number,

$$Re_\theta = \frac{U_\infty \theta}{\nu}.$$

Equation 2

Here U_∞ is the freestream velocity. One of the primary objectives for this water tunnel was to achieve a turbulent boundary layer with a Re_θ value of at least 10^4. The following sub-sections describe the theoretical approach used to estimate the Re_θ for given test section configurations in order to obtain initial sizing of the test section.

3.1 Test Section Sizing

The test section sizing was conducted in two phases. Initially, no pressure gradient was assumed. The results from this approach were then further confirmed by calculating a non-dimensional acceleration parameter that accounted for local flow acceleration. The analysis and results for each of these phases are discussed in the following sub-sections.

3.1.1 Flat plate analysis assuming zero pressure gradient

Even though the actual test section will experience a pressure gradient due to the confined space and a growing boundary layer, initial estimates assumed no pressure gradient. For the test section, an initial maximum speed of 10 m/s was considered based on cavitation concerns. For speeds above 10 m/s, the chances of cavitation are high and small disturbances in the flow stream could easily lead to cavitation. The test section length was limited to 1 m due to concerns related to manufacturability and test section rigidity. Based on established facilities, this value should result in the fabricated structure being sufficiently rigid, flat and smooth. The working fluid was assumed to be water at room temperature.

Following the momentum-integral analysis of White (2006) for a turbulent boundary layer on a flat plate with zero pressure gradient and an initial momentum thickness of zero, if a one-seventh velocity profile is assumed, the boundary layer thickness can be approximated as

$$\frac{\delta}{x} = 0.16 Re_x^{-1/7}$$

Equation 3

where x is the downstream distance from the leading edge of the flat plate and δ is the boundary layer thickness . For a one-seventh velocity profile, the boundary layer thickness can be related to the displacement thickness (White, 2006)

$$\frac{\theta}{\delta} \approx \frac{7}{72}.$$

Equation 4

Eq. 3 and Eq. 4 can be combined to obtain a relationship between displacement thickness and downstream distance.

$$\frac{\theta}{x} = 0.015\left(\frac{UX}{\nu}\right)^{-1/7}$$

Equation 5

The above equation can be non-dimensionalized to obtain a relationship between Re_θ and x.

$$Re_\theta = 0.015\left(\frac{UX}{\nu}\right)^{6/7}$$

Equation 6

The above equation can now be used to plot Re_θ along the length of the test section. It can be seen from Figure 4 that for a 1 m long test section with a water flow speed of 10 m/s, Re_θ of 10^4 is achieved at a downstream distance of 0.57 m. However, this calculation does not account for flow non-uniformities and assumes no turbulence. Figure 4 also shows that a 1m long test section will be able to achieve Re_θ value of over 10^4, the initial design requirement.

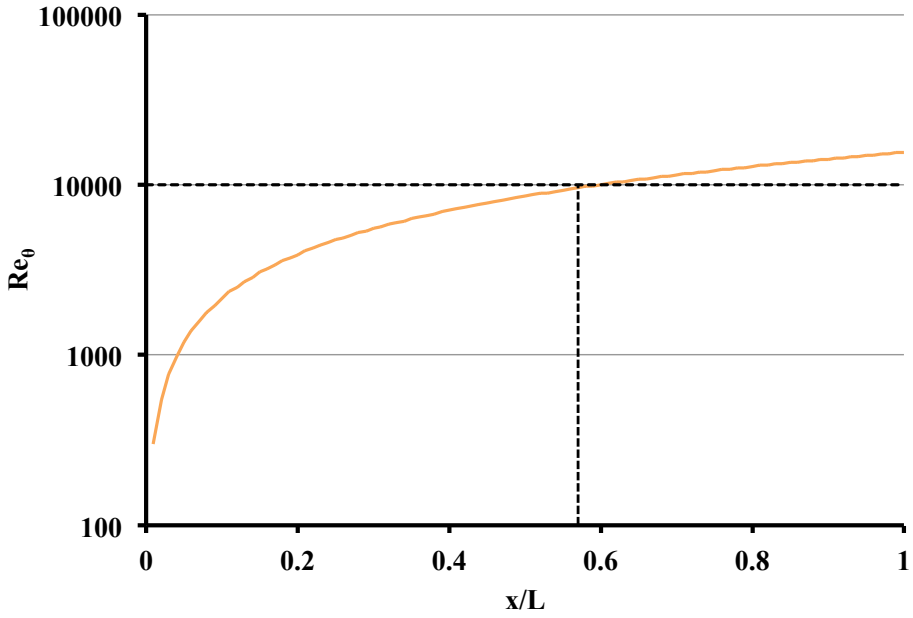

Figure 4: The momentum-thickness based Reynolds number as a function of downstream distance normalized with the test section length. Estimates were made assuming a zero-pressure-gradient flat plate with a free-stream speed of 10 m/s. Dashed lines mark the tunnel design condition of $Re_\theta = 10^4$.

Based on previously mentioned limits and assumptions, the boundary layer thickness can be approximated as follows:

$$\frac{\delta}{x} = 0.16 Re_x^{-1/7} = 0.16 * \left(\frac{10 \frac{m}{s} * 1\ m}{\frac{10^{-6} m^2}{s}} \right)^{-\frac{1}{7}} = 0.16 * (10^7)^{-\frac{1}{7}} = 0.016$$

Equation 7

Thus, for a 1 m long test section, the boundary layer thickness at the end of the test section is estimated to be 16 mm. The validity of the zero pressure gradient assumption is valid when the boundary layer thickness is sufficiently small compared to the test section height. This also assures the boundary layers from the walls are not going to merge and create a channel flow in the test section. Thus if it is assumed that the test section height (h) should be at least 10 times the boundary layer thickness, an estimate of the required test section height can be produced.

$$\frac{\delta}{h} < 1/10 \rightarrow h > 10\delta \approx 0.16\, m = 6.3\, inches$$

Equation 8

The boundary layer is the thickest at the end of the test section. As a result, the test section height is based on the worst-case scenario. This resulted in a minimum height requirement of roughly 160 mm (6.3 in). However, in order to keep costs down, it was desirable to minimize the initial guess for the test section height. A 6 in. square cross section was chosen as the initial guess for the test section height. In the next sub-section, the effect of the pressure gradient on this 6 in. square cross-section is computed in order to ascertain that the pressure gradient is weak and that the turbulent boundary layer is not affected by this pressure gradient.

3.1.2 Effect of pressure gradient on turbulent boundary layer

The previous section assumes no pressure gradient in the flow over the flat plate. However, in the actual test section, local acceleration (dU/dx) will exist due to the presence of a growing boundary layer on all four surfaces of the test section. Conserving mass and including the effect of the wall boundary layers using the displacement thickness can capture the effect of the growing boundary layer.

$$U_e A = U(x)(A - P\delta^\star)$$

Equation 9

Here U_e is the initial freestream velocity at the leading edge of the test section, A is the cross sectional area, P is the perimeter and $\delta^\star$ is the boundary layer displacement thickness. For a square cross section and a boundary layer that follows the one-seventh velocity profile, this equation can be reduced:

$$U(x) = \frac{U_e}{1 - (\frac{4\delta^\star}{h})} = \frac{U_e}{1 - (\frac{\delta}{2h})} = \frac{U_e}{1 - \left(\frac{0.16xRe_x^{-1/7}}{2h}\right)}$$

Equation 10

In order to assess the strength of the resulting pressure gradient within the test section, another dimensionless acceleration parameter (*K*) is computed, which is defined as

$$K = \frac{\nu}{U_e^2}\frac{dU}{dx}.$$

Equation 11

This parameter quantifies the pressure gradient indirectly by computing the velocity gradient, which is directly related to the pressure gradient in the streamwise direction. The velocity gradient can be obtained by differentiating Eq. 10 as shown below:

$$\frac{dU}{dx} = \frac{d}{dx}\left(\frac{U_e}{1 - \frac{0.08xRe_x^{-1/7}}{h}}\right) = \frac{d}{dx}\left(\frac{U_e}{1 - \frac{0.08}{h}\frac{x^{6/7}}{(U_e/\nu)^{1/7}}}\right)$$

$$\frac{dU}{dx} = U_e \frac{\frac{0.08}{h}\frac{6/7x^{-1/7}}{(U_e/\nu)^{1/7}}}{\left(1 - \frac{0.08}{h}\frac{x^{6/7}}{(U_e/\nu)^{1/7}}\right)^2}$$

Equation 12

Eq. 12 can be then incorporated into Eq. 11 to provide a value of *K* that is only dependent on the test section height, the initial free-stream velocity, the viscosity of the fluid and the downstream distance.

$$K = \frac{\frac{0.069}{hx^{1/7}}\left(\frac{\nu}{U_e}\right)^{8/7}}{\left(1 - \frac{0.08x^{6/7}}{h(U_e/\nu)^{1/7}}\right)^2} = \frac{\frac{0.069}{hRe_x^{1/7}}\frac{\nu}{U_e}}{\left(1 - \frac{0.08x}{Re_x^{1/7}h}\right)^2}$$

Equation 13

For a given free stream speed and kinematic viscosity, the above equation allows the plotting of this parameter along the test section length. The corresponding non-dimensional plot, for a velocity of 10 m/s, is shown in Figure 5. The classical turbulent boundary layer log law remains unaffected for $K < 1.62\times10^{-6}$ (Patel, 1965). Figure 5 shows that the calculated K values are more than two orders of magnitude lower than this criterion. As a result, it is expected that the turbulent boundary layer will not be affected by the pressure gradient present along the test section, which indicates that the original zero-pressure gradient flat plate analysis was valid.

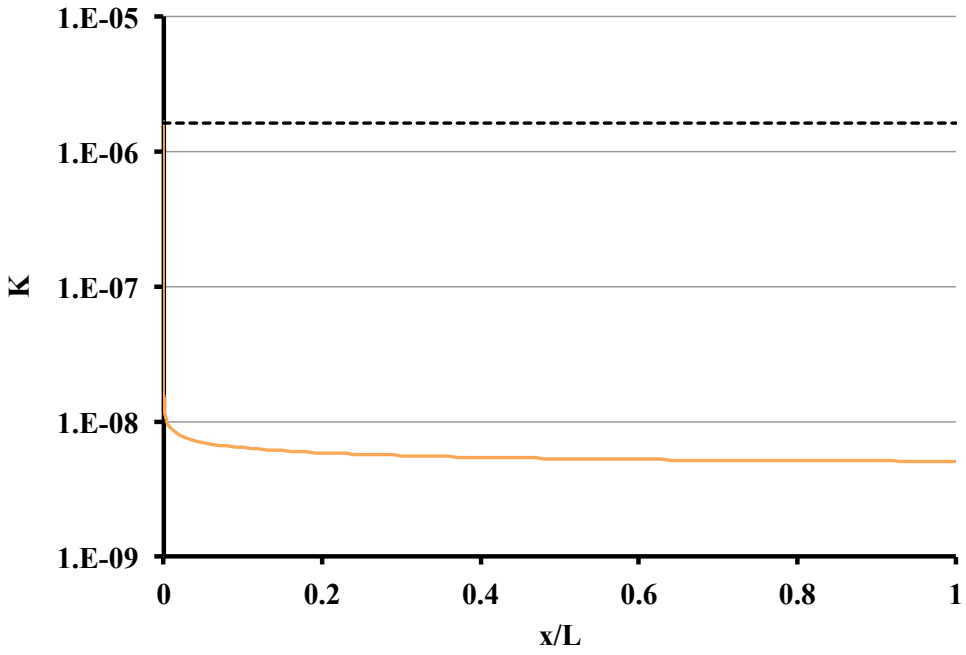

Figure 5: Estimates of non-dimensional acceleration parameter *K* plotted as a function of downstream distance (*x*) normalized with the test section length (*L*).

3.1.3 Surface Roughness

The surface roughness of the test surface directly impacts the amount of turbulence generated in the test section. A parameter, k^+, relates surface roughness to turbulence length scale (White, 2006), as shown in Eq. 14.

$$k^+ = \frac{k}{l_\mu}$$

Equation 14

Here l_μ is the viscous wall unit, which is the characteristic length within the viscous sublayer and is defined as

$$l_\mu = \frac{\nu}{u_T} = \frac{\nu}{\sqrt{\frac{\tau_w}{\rho}}} = \frac{\nu}{\sqrt{\frac{C_f \rho U^2}{2\rho}}} = \frac{\nu}{U}\left(\frac{C_f}{2}\right)^{-1/2}.$$

Equation 15

Here u_T is defined as the friction velocity.

Since the flow speed, *U*, is known and if a zero pressure gradient flat plate condition is assumed, C_f can be calculated, an estimate can be made for the characteristic viscous length, l_μ. A k^+ value of 4 or lower is desirable for a smooth surface (White, 2006). Based on the values of l_μ, estimates can be made for the maximum allowable surface roughness, k, as shown in Figure 6.

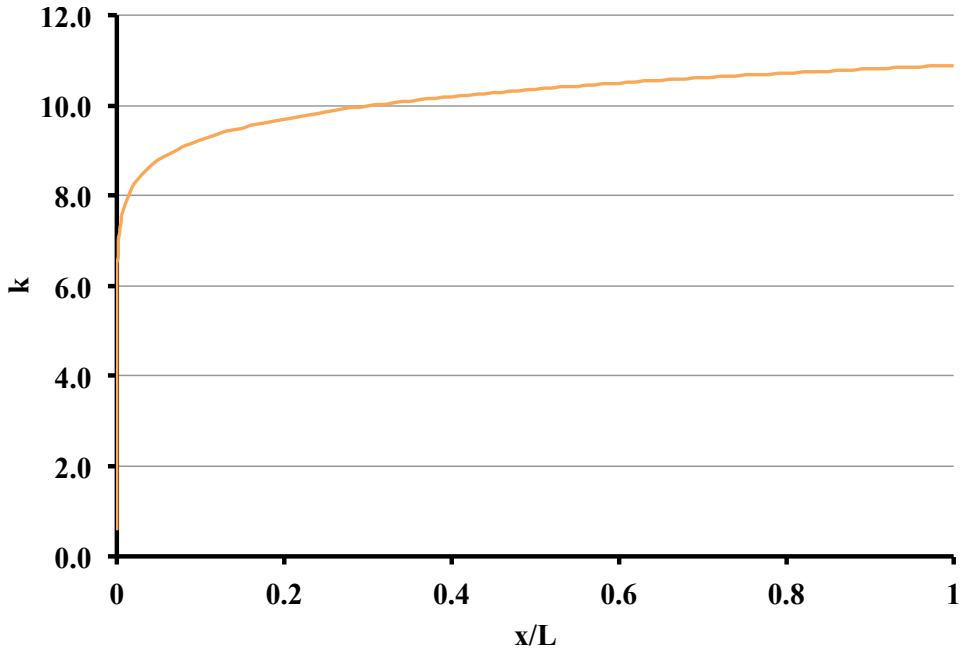

Figure 6: Estimate for maximum surface roughness for a hydrodynamically smooth plate ($k^+ \leq 4$) plotted as a function of the normalized test section downstream distance.

This roughness estimate translated to a roughness RMS value of 8-10 microns (roughly 350 microinches) and an ISO Grade Number N10 for machining purposes (Jerz, 2006). An ISO Grade Number N10 machining requirement is much rougher than what is typical for machinists. As a result, a N6 machining finish (32 microinches) will be utilized, which will produce a sufficiently smooth surface (Jerz, 2006). This machining finish translated to an average k^+ value of 0.3 at a freestream speed of 10 m/s. This is much lower than the criterion used in White (2006) and even smaller than the most conservative requirements for a hydraulically smooth surface ($k^+ < 1$). The corresponding values of k^+ along the test section length are shown below in Figure 7.

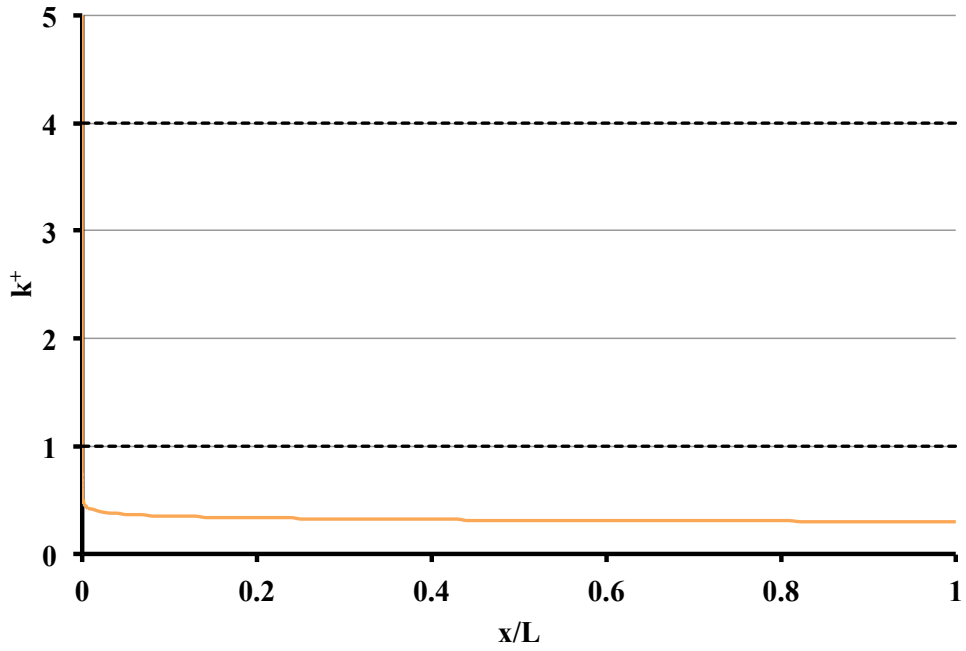

Figure 7: Estimated inner variable scaled surface roughness k^+ along the test section length with the prescribed surface finish (N6).

3.2 Test Section Design/Layout

This section describes the various components of the test section. The individual components are described, along with the sizing routine that was employed for the bolt spacing, O-ring sizing and thickness estimates for the acrylic and stainless steel components. An isometric view of the test section is shown in Figure 8.

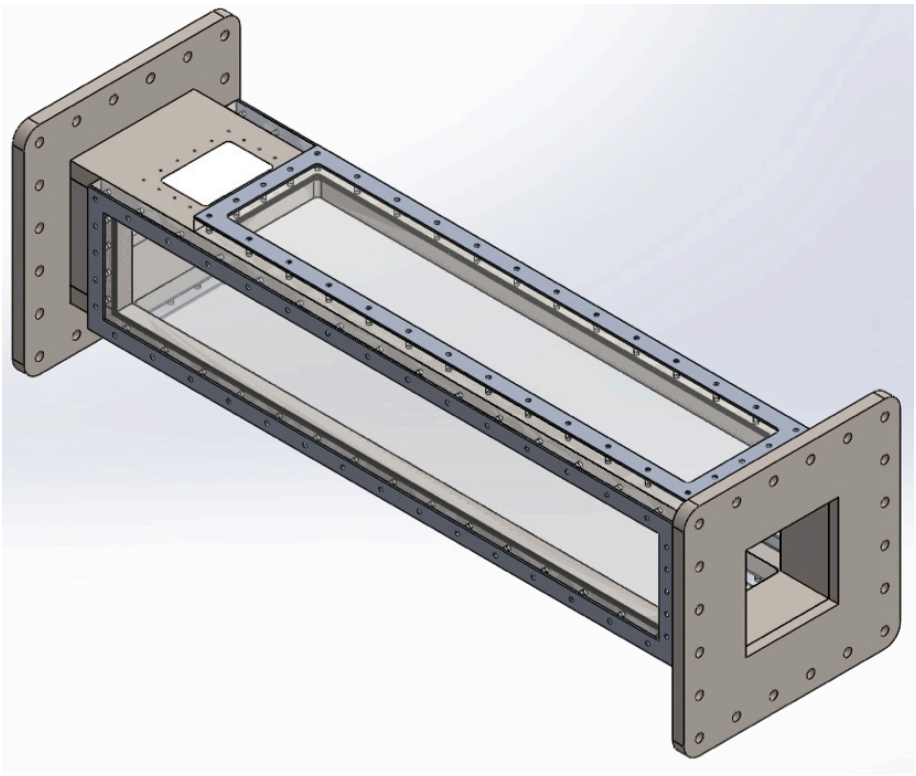

Figure 8: Isometric view of the as designed test section including the stainless steel frame and acrylic windows.

The test section shown in Figure 8 is comprised of 17 individual components. Detailed technical drawings of each component of the test section and the instructions for the assembly of the test section (weld placement) can be found in Appendix A.

3.2.1 Test Section Skeleton

The stainless steel test section skeleton consists of the top frame, bottom frame, the four spreaders and the two flanges as shown in Figure 9.

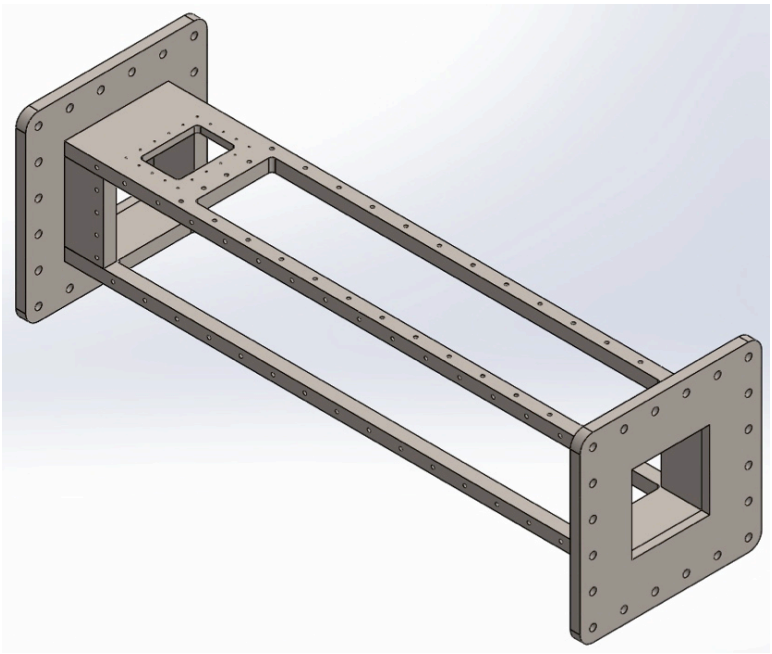

Figure 9: Test section "skeleton", which consists of the stainless still frame.

The top and bottom frame are cut from 1-inch thick solid stainless steel plates. The stainless steel spreaders are surface welded to these frames at the junctions. There is 3-inch of metal available on both weld junctions to allow proper heat dissipation and to minimize warping during the welding process. This frame is then welded to the two flanges, to create the skeleton frame as shown in Figure 9.

The 8-inch × 8-inch recess in the flange holds the rest of the test section skeleton in place during the weld process. Surface welds at the flange and frame intersection holds the test section skeleton in place. These welds are 100% sealed in order to avoid water leakage when the test section in pressurized. (See Appendix A for weld locations).

The ¼-inch boltholes are tapped into the skeleton. The hole-depth is ½-inch and the holes are tapped up to a distance of 3/8-inch. The holes are spaced 2.5 inch apart and are staggered in

order to avoid intersection of the boltholes. Each side of the test section skeleton is bolted to an acrylic plate and an aluminum cover plate. These components are detailed in the next two sub-sections.

An FEA simulation, using a commercial software (SolidWorks Simulation, Dassault Systèmes), of the top plate was conducted to analyze any potential structural issues. The top plate was chosen as the critical component because of its complicated design as compared to the other pieces of the skeleton. The FEA simulation was based on a constant gauge pressure loading of 40 psi on the inner face. The top face was held in position and not allowed to move. This is representative of the operational situation. The results from this FEA simulation are shown in Table 2.

Table 2: FEA simulation results for the top frame with a 40 psi pressure difference.

Thickness (in.)	1.0
Yield Strength (MPa)	172.37
Max. Von Mises Stress (MPa)	0.71
Max. Displacement (nm)	48
Max. Strain (με)	2
Factor of Safety	243.6

3.2.2 Top, Bottom and Side Acrylic Plates

The test section plates or windows are machined out of 1.75-inch thick acrylic sheets. The holes on the test section plates are machined to match the test section skeleton holes. The side plates are interchangeable. The O-ring grooves are also machined on the acrylic plates due to space constraints on the stainless steel frames.

FEA simulations, using a commercial software (SolidWorks Simulation, Dassault Systèmes), of the loading on the acrylic plates were conducted to ensure structural integrity under a uniform gauge pressure loading of 40 psi. The simulation was done on the most critical acrylic part, the bottom plate. The bottom plate was chosen as the most critical part since it has the largest surface area, and will thus experience the largest force. A 40 psi pressure load was applied to the inside face of the bottom surface, while the outside surface was held in position. This reflected the operational environment where the bottom plate will be held in place by the bolts and only the inside face will be in direct contact of the pressure load. The results from these simulations are shown in Table 3.

Table 3: FEA simulation results for the bottom plate with a 40 psi pressure difference.

Thickness (in.)	1.75
Yield Strength (MPa)	45.00
Max. Von Mises Stress (MPa)	10.60
Max. Displacement (nm)	114900
Max. Strain (με)	2550
Factor of Safety	4.2

3.2.3 Aluminum Cover Plates

The cover plates are made out of 1/8-inch thick aluminum sheets. The plate allows even distribution of the internal pressure load instead of creating point loads on the acrylic plates at the bolt locations. The cover plates are designed to allow visualization of the wall when viewed from the side. This allows PIV studies near the wall region without the need for light refraction using a prism. Since the cover plates did not come in contact with the flow stream, corrosion was not a concern and thus aluminum was chosen as the material because of its availability, weight and ease of fabrication.

3.2.4 Top Injector Plate

A 4.5-inch by 3-inch top injector plate was designed as part of the test section to allow dye or polymer injection within the turbulent boundary layer. This plate will be used as a filler piece during experiments that do not require injection. The top injector plate bolts onto the top frame using eighteen 1/8-inch bolts. An O-ring groove on the top frame assures no leakage at this junction. The flow surface has a surface finish of 0.81 μm (32 μin), which is sufficient to consider the injector surface hydraulically smooth.

3.2.5 Flanges

The flanges are designed to allow smooth mating surfaces between the test section and the contraction/diffuser sections. The hole-pattern on the test section flanges are matched with the flanges on the contraction and diffuser sections. A gasket is placed at these junctions in order to prevent water leakage. The flanges are designed with a 1/8-inch recess to hold the test section frame skeleton in place during the welding process. An O-ring groove is also part of the design in order to assure no leakage occurs at the flange and frame junctions. The flanges also connect the test section to the support structure and the optical table, as discussed later.

3.2.6 Bolt Spacing and Sizing

The test section skeleton and the acrylic plates are held in place using bolts. These bolts go through the cover plates, acrylic plates and have 3/8-inch contact with the stainless steel frame. These bolts hold the test section together when it is pressurized. The bolts are 1-1/8 inch long. The sizing of the bolt diameters is based on the pressure experienced within the test section. In order to calculate the stress (axial and shear) on each bolt, the following equations were used:

$$F = PA$$

Equation 16

$$\sigma = \frac{F_b}{\pi \frac{d_b^2}{4}} = \frac{NF}{\pi \frac{d_b^2}{4}} = \frac{NPA}{\pi \frac{d_b^2}{4}}$$

Equation 17

$$\tau = \frac{F_b}{\frac{\pi}{2}(d_{b-}\, 0.064952/n_b) l_b} = \frac{NPA}{\frac{\pi}{2}(d_{b-}\, 0.064952/n_b) l_b}$$

Equation 18

Here F is the total force on the test surface, P is the pressure exerted on the test surface, A is the area of the wetted surface, F_b is the force per bolt, N is the total number of bolts, d_b is the bolt diameter, n_b is the number of threads per inch, l_b is the contact length, σ is the axial stress experienced by each bolt and τ is the shear stress experienced by each bolt.

The test section will be pressurized to a maximum pressure of 40 psi. The number of bolts was based on a bolt spacing of 2.5 inch. This bolt spacing was based on space constraints, design standards (AISC, 2005) and recommendations from other test section designs (Nedyalkov, 2012). The resulting forces are tabulated in Table 4. For a 1/4 inch Grade 5 bolt, the proof load is 85,000 psi (Tessco, 2014). This led to a minimum factor of safety of 18.35, as shown in Table 4.

Table 4: Bolt sizing and the expected loading at 40 psi.

Part	*P* (psi)	*F* (lb.)	*N*	σ (psi.)	τ (psi.)	Proof Load (psi.)	Factor of Safety
Side Plate	40	8640	39	4513.14	762.09	85,000	18.83
Bottom Plate	40	8640	38	4631.91	782.15	85,000	18.35
Top Plate	40	7200	32	4583.66	774.00	85,000	18.54

3.2.7 *O-Ring Sizing*

Based on space constraints on the acrylic plates and availability, a suitable O-Ring width was chosen. The groove depth is defined by the amount of desired squeeze,

$$c_d = w - \frac{w - squeeze_d}{100}.$$

Equation 19

Here c_d is the desired groove depth, *w* is the O-ring width and $squeeze_d$ is the desired percentage of squeeze. Optimal squeeze for a face seal application is 30% (Parker Handbook, 2007). The O-Ring groove width (*g*) is based on recommendations from the Parker Handbook (2007) for the face seal application. The results are shown in Table 5.

Table 5: O-Ring Groove Sizing

O-ring width	*w*	0.139
Desired Squeeze	$squeeze_d$	30%
Groove depth	c_d	0.0973
Groove width	*g*	0.187
O-ring Area	A_O=*pi*w^2/4*	0.0152
Groove Area	A_g=c_d**g*	0.0182
Area Ratio (%)	A_O/A_g**100*	83

3.2.8 *Test Section Corner Design Concerns*

Based on the comparative study done by Nedyalkov (2012), it was decided that a simple 90° corner would not introduce significant amount of three-dimensionality within the test section. In the comparative study, calculations showed that a 1" fillet on all the corners would produce higher centerline velocity variation as compared to no fillets (i.e., 13.5% with fillets as compared to 12.7% without fillets). Reasonable reduction in velocity fluctuation was only observed for diminishing fillets (6.4%). However, this design would not be cost effective. Moreover, the design would not be advantageous towards the end of the test section. Both fillet designs

prevented direct optical access to the flow surfaces. Based on the objectives for this facility, the advantage of having direct optical access to the wall outweighed the expected impact of corner flows within the test section. Additionally, these corner cross flows are only localized in the absence of flow separation (Bell and Mehta, 1988). The test section is not expected to have any kind of flow separation. As a result, it was decided to not use the fillets.

CHAPTER IV

FLOW CONDITIONING

The type of flow conditioning used in the water tunnel loop heavily influences the flow quality in the test section, especially at high Reynolds number. This section delineates the design routine employed for the turbulence management and flow straightening components, namely, honeycomb section, settling chamber and contraction section.

4.1 Honeycomb and Settling Chamber Sizing

The honeycomb section is the main flow-conditioning unit for this water tunnel loop. The honeycomb section is placed before the settling chamber. This position was chosen to minimize the turbulence intensity in the test section by allowing turbulent decay of the flow behind the honeycomb cell. The purpose of the honeycomb section is to remove swirl from the flow (i.e. straighten the flow) and breakup large turbulent structures.

The honeycomb sizing was based on the work of Lumley and McMahon (1967). The primary results of interest from this work are summarized in two figures, which are reproduced here in Figure 10. These figures were used as sizing charts to obtain the final honeycomb cell dimensions for the current facility.

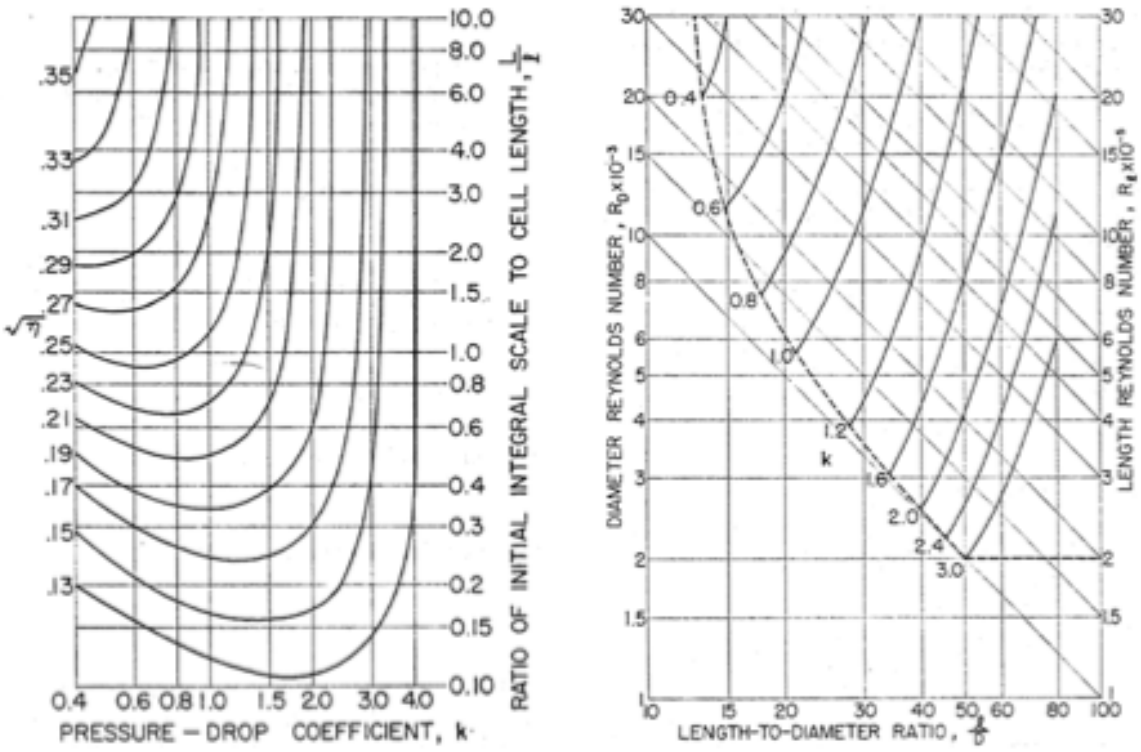

Figure 10: Figures from Lumley and McMahon (1967) that were used in the current study to size the honeycomb sections. Shown are (left) a isoreduction contour plot and (right) a pressure drop contour plot.

The turbulence reduction factor η, shown in the left plot of Figure 10, is a measure of the turbulence suppression. It is defined as the ratio of the velocity fluctuations downstream and upstream of the honeycomb section,

$$\eta = \frac{\left(\overline{u^2}\right)_{downstream}}{\left(\overline{u^2}\right)_{upstream}}.$$

Equation 20

Here u is the fluctuating velocity component either upstream or downstream of the honeycomb and the overbar indicates that it is the average value. It is desirable to have the lowest value for η because an objective for this design is to minimize the turbulence within the test section. The pressure drop coefficient (k), shown in Figure 10, is defined as

$$k = \frac{\Delta p}{0.5\rho U^2}.$$

Equation 21

Here Δp is the pressure drop experienced across the honeycomb section, ρ is the density of the fluid and U is the flow speed past the honeycomb section. It is desirable to have a low k value in order to minimize the pressure head loss. A higher head loss would require a bigger pump and motor.

The isoreduction contours from Figure 10 (left) represents the performance characteristics of the honeycomb section. It can be seen that for each contour line, there is a pressure drop coefficient, k, above which the performance of the honeycomb section is quite unstable. As a result, it is desirable to have a k value lower than this critical value. However, for the lowest pressure drop coefficients on a contour line, it can be seen from Figure 10 (right) that the range of acceptable length to diameter ratio is narrower. This limits the design space of the honeycomb. As a compromise, the starting point was chosen as the minima on the lowest contour line, corresponding to a $\sqrt{\eta}$ value of 0.13.

In Figure 10 (left), the minimum value of $\sqrt{\eta}$ contour line of 0.13, provides a pressure drop coefficient, k, of roughly 2.0 and a L/l value of 0.10. The integral turbulence length scale (L) is defined as the measure of the largest turbulent structure in the flow stream. As an initial estimate for the current facility, half the inlet diameter to the honeycomb section was used as a conservative approximation, which is nominally 10 in. This results in a honeycomb section length (l) of 200 in and a honeycomb length based Reynolds number (Re_l) of 58.2×10^5. This data point is not within the data range shown in Figure 10 (right). It is desired to avoid extrapolation of the

data provided by Lumley and McMahon (1967) in order to prevent unpredictable performance characteristics. As a result, a $\sqrt{\eta}$ value of 0.13 is not a desirable design choice. A similar procedure is performed on the next contour line ($\sqrt{\eta}$ =0.15) in Figure 10 (left). This design routine is iterated until a minimum isoreduction factor is attained along with the honeycomb cell dimensions that lie within the data range shown in Figure 10 (right) is has a stable isoreduction factor.

The final $\sqrt{\eta}$ value is 0.19, with a pressure-drop coefficient, *k*, of 1.0. This translated to a L/l of 0.35. For a *L* value of 10 in., a honeycomb length (*l*) of 28.5 inches is calculated. This resulted in a Re_l of 11.6×10^5 and length to diameter ratio (*l*/*D*) of roughly 36. This translated to a cell diameter of 0.79 inches. However, based on manufacturability limitations, a final hexagonal cell diameter (*D*) of 0.75 inches (0.019 m) and a honeycomb length (*l*) of 24 inches (0.61 m) were chosen. This provided a honeycomb design with a pressure drop coefficient, *k*, of 0.9 and a turbulence reduction factor, $\sqrt{\eta}$, of roughly 0.2.

For the honeycomb cell diameter (*D*) of 0.019 m and a flow speed (*U*) of 1.14 m/s (based on mass conservation and a 10 m/s test section speed), a diameter based Reynolds number can be calculated as

$$Re_D = \frac{DU}{\nu} = \frac{(0.019\ m) * (1.14\ m/s)}{(10^{-6}\ m^2/s)} = 21829.$$

Equation 22

This Reynolds number describes a turbulent pipe flow since the Re_D value is above 2000 (White, 2006). Wetzel and Arndt (1994) describes the turbulence level behind a honeycomb cell as a

combination of viscous decay of the turbulent flow and the reduced turbulence because of the honeycomb's turbulence reduction factor, as shown in Eq. 23.

$$\left(\frac{\overline{u^2}}{\overline{U^2}}\right)_P = \frac{0.0072}{x/D} + \eta\left(\frac{\overline{u^2}}{\overline{U^2}}\right)_I$$

Equation 23

Here u is the velocity fluctuation component, U is the freestream velocity, x is the distance downstream of the honeycomb section, P denotes the plenum location downstream of the honeycomb and I denotes the honeycomb inlet location. A length of 35 in. was chosen for the settling chamber. This dimension was limited by the lab space available. This settling chamber length is used for the viscous decay of the turbulent flow behind the honeycomb section and is higher than the recommended minimum length of 30-40 cell size as suggested by Loehrke and Nagib (1976). If an incoming turbulence level of 13% is assumed (Wetzel and Arndt, 1994), Eq. 23 can be used to obtain the velocity fluctuation level at the settling chamber outlet (or the contraction inlet):

$$\left(\frac{\overline{u^2}}{\overline{U^2}}\right)_P = \frac{0.0072}{35/.75} + 0.2^2 * 0.13^2 = 0.00083$$

Equation 24

The effect of contraction on turbulence suppression was described by Batchelor (1960) using Eqs. 25-27.

$$\left(\frac{\overline{u^2}}{\overline{U^2}}\right)_T = \frac{\mu + 2\nu}{3c^2}\left(\frac{\overline{u^2}}{\overline{U^2}}\right)_P$$

Equation 25

$$\mu \cong \frac{3}{4c^2}(\log(4c^3) - 1)$$

Equation 26

$$\nu \cong \frac{3}{4}c$$

Equation 27

Here c is the contraction ratio of the nozzle, μ and ν are functions of contraction ratio that accounts for the nonisotropy of the turbulence. For a contraction ratio of 8.5:1 and the turbulence created by the honeycomb, denoted by Eq. 24, a minimum turbulence level intensity at the test section can be obtained, as shown by Eq. 28, were T is the outlet location of the contraction (or the test section inlet).

$$\sqrt{\left(\frac{\overline{u^2}}{\overline{U^2}}\right)_T} = \sqrt{0.0589\left(\frac{\overline{u^2}}{\overline{U^2}}\right)_P} = \sqrt{0.0589 * 0.00083} = \sqrt{0.000049} = 0.70\%$$

Equation 28

The water tunnel flow loop employs a centrifugal pump and four 90° elbows. These components will lead to significant swirl and velocity fluctuations to the flow stream, especially at high speeds. As a result, the incoming turbulence intensity (*TI*) level is expected to be higher than the axial pump and vaned elbows configuration that provided a 13% inlet *TI* value (Wetzel and Arndt, 1994). During operation, if the turbulence intensity in the test section is higher than desirable, the following design changes can be made to reduce the turbulence level in the test section:

- Add screens or an additional honeycomb section to break down the swirling flow and reduce the size of the largest turbulent structures at the honeycomb inlet section. It can be seen from Figure 11 that there is a significant reduction in the TI levels in the test section with a reduction in the inlet TI levels at the honeycomb section.

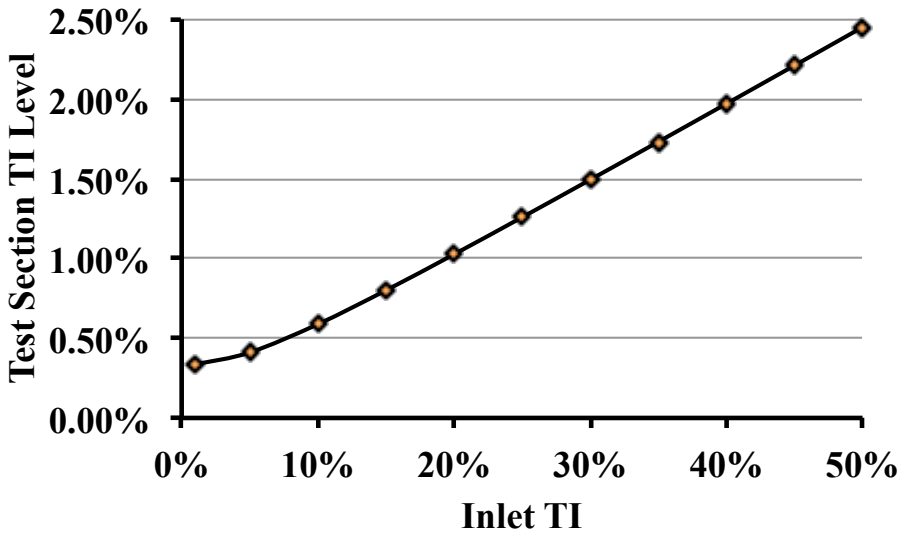

Figure 11: Test section TI levels as a function of the TI levels at the inlet to the honeycomb.

- Reduce the honeycomb cell size. This reduces the viscous decay factor, thereby reducing the turbulence level in the test section, as seen in Eq. 23. If a honeycomb cell size lower than 0.5 in. is utilized, the TI values are reduced considerably as shown in Figure 12.

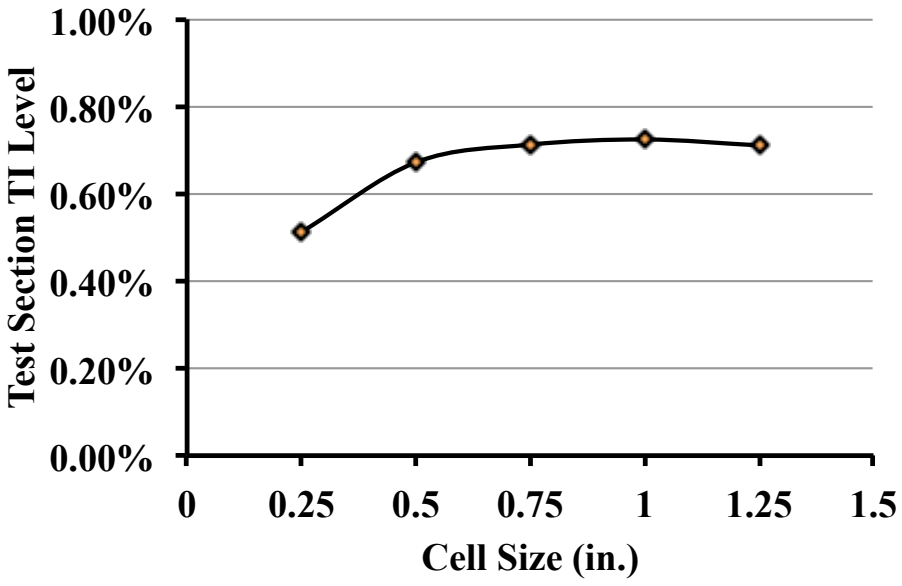

Figure 12: Effect of honeycomb cell size on the test section TI levels.

- Increase the contraction ratio. This will reduce the velocity fluctuation levels at the contraction inlet as seen in Eq. 25. The effect of increasing contraction ratio on the test section TI levels is pretty weak, as can be observed from Figure 13. Moreover, this will be a very expensive modification because the complete flow loop will have to be modified along with the support structure.

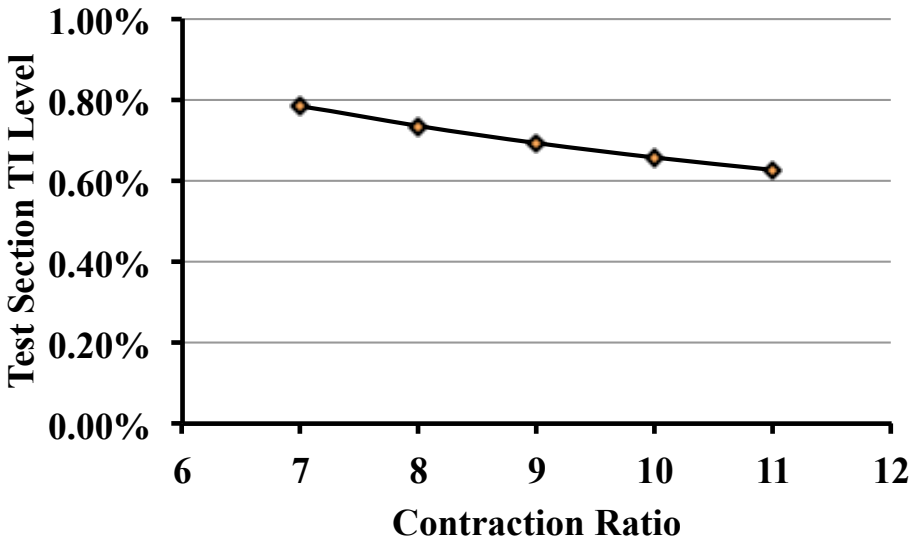

Figure 13: Effect of contraction ratio on the test section TI levels.

4.1.1 Secondary Honeycomb Section (HC2) Sizing

In order to further reduce the TI levels in the test section, it was decided that a second honeycomb section (HC2) should be installed downstream of the original honeycomb section (HC1) as described in the previous section. This decision was based on the results from Figure 11 and Figure 12, which show a potential for considerable reduction in test section TI if a second honeycomb section is suitably sized.

Since the cell size of HC1 was around 0.75 in., it was deemed satisfactory to reduce the cell size of HC2 to 0.25 in. or lower, based on the roll-off observed in Figure 12. Honeycomb sizing charts from Figure 10 can be utilized to size the HC2 section. For HC2, a sizing procedure similar to HC1 was repeated. However, the upper limit on the diameter was fixed at 0.25". The integral length scale (L) for the HC2 section will be in the order of 0.75 in. since the flow is downstream of HC1 with a cell size of 0.75 in.

The final honeycomb sizing dimensions were a cell size (D) of 0.25 in. and a length (l) of 6 in. This provides a $\sqrt{\eta}$ value of 0.13 and a pressure drop coefficient, k, of 1.0. A 6 in. long HC2 section provides 29 in. for the settling chamber length, which is within the 30-40 cell sizes length recommendation from Loehrke and Nagib (1976) for a 0.25 in. cell size. Using superposition, the effect of the two honeycomb sections can be combined in order to obtain a combined turbulence reduction factor for the two honeycomb sections (HC1 and HC2).

$$\sqrt{\eta} = \sqrt{\eta_{HC1} * \eta_{HC2}} = 0.2 * 0.13 = 0.026$$

Equation 29

Eq. 23 and Eq. 28 can now be used to estimate the test section TI levels as function of the inlet TI values because of the presence of the two honeycomb sections (HC1 and HC2), a 29 in. long settling chamber and an 8.5:1 contraction ratio. The final relationship between the test section TI levels and the incoming turbulence levels is described using Eq. 31.

$$\left(\frac{\overline{u^2}}{\overline{U^2}}\right)_P = \frac{0.0072}{x/D} + \eta\left(\frac{\overline{u^2}}{\overline{U^2}}\right)_I = \frac{0.0072}{29/0.25} + 0.026^2\left(\frac{\overline{u^2}}{\overline{U^2}}\right)_I = \left(6.21 + 67.6\left(\frac{\overline{u^2}}{\overline{U^2}}\right)_I\right)\times 10^{-5}$$

Equation 30

$$Test\ Section\ TI = \sqrt{\left(\frac{\overline{u^2}}{\overline{U^2}}\right)_T} = \sqrt{0.0589\left(\frac{\overline{u^2}}{\overline{U^2}}\right)_P} = \sqrt{0.036 + .40\left(\frac{\overline{u^2}}{\overline{U^2}}\right)_I}\ \%$$

Equation 31

This relationship can be plotted as shown in Figure 14. It is important to note that the addition of a second honeycomb section (HC2) reduced the turbulence level from 0.7% to 0.21%, for an incoming TI level of 13%. The two honeycomb sections also weaken the effect of the inlet TI level on the test section TI level. This can be inferred by analyzing the shallower slope of Figure 14 as compared to the slope from Figure 11. This is beneficial since an accurate measurement for the inlet TI values is not available. However, from Figure 14, it can be inferred that the test section TI values should be close to 0.35%, half of the initial TI estimate based on one honeycomb section (HC1 only), even if the inlet TI levels are as high as 50%.

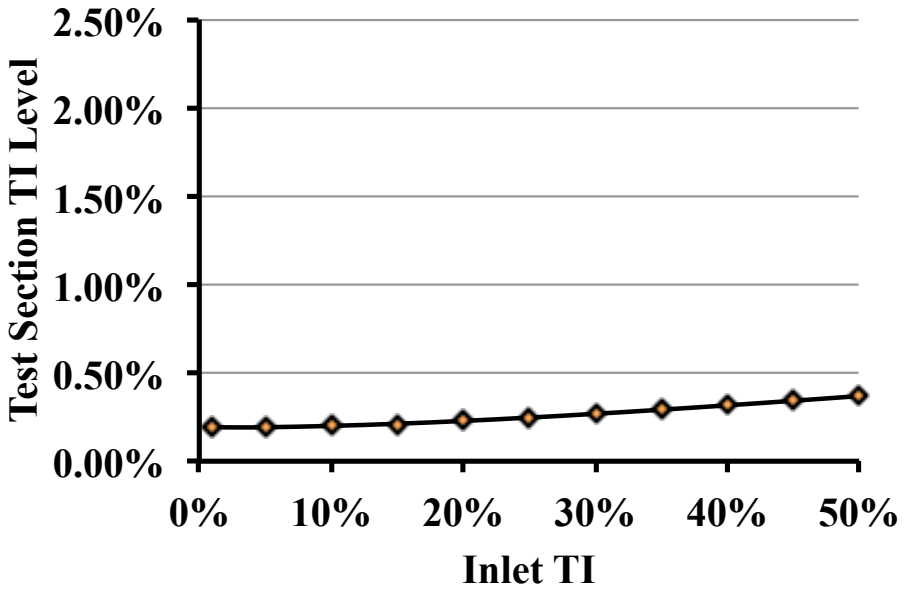

Figure 14: Relationship between test section TI levels and incoming TI levels.

4.2 Contraction

The main purpose of the contraction section is to reduce the turbulence intensity, while increasing the flow speed. This is achieved by a sudden reduction in the cross sectional area. The following section discusses the approach utilized for the design of the contraction section.

4.2.1 Profile shape

A schematic of a typical contraction profile is shown in Figure 15. In Figure 15, Y_O and Y_I are the ordinates measured from the test section centerline at the contraction outlet and inlet, respectively, and L is the total length of the contraction. Horizontal dimension, X, is defined as decreasing in the downstream direction and vertical dimension, Y, is defined as increasing in the upward direction. The terms, Y_C and X_C are non-dimensional parameters defined as

$$Y_C = (Y - Y_O)/(Y_I - Y_O) \text{ and}$$

Equation 32

$$X_C = X/L$$

Equation 33

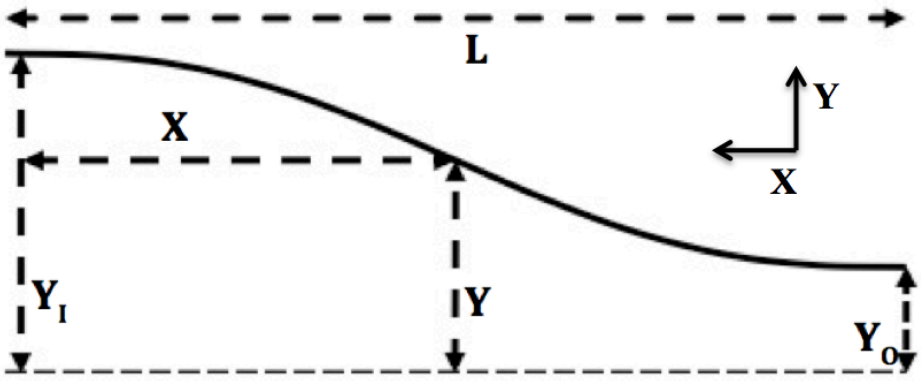

Figure 15: Schematic of a typical contraction profile, which can be fitted to a fifth order polynomial.

It was noted by Bell and Mehta (1988) that a 5th order polynomial curve is a good fit for a contraction profile. Some of the pre-existing facilities that use the 5th order polynomial curve fit for the contraction section include the LCC (Etter, 2006), HYKAT (Arndt and Weitendorf, 1990) and LOCAT (Wosnik and Arndt, 2006). A 5th order polynomial requires six independent boundary conditions to produce a solution, which are determined from constraints at the inlet and outlet:

1. The inlet and outlet sizes must match the test section and given contraction ratio, which can be expressed as $Y_C(0) = 0$ and $Y_C(1) = 1$.
2. The slope at the inlet and outlet should be equal to zero to minimize flow disturbances and promote uniform straight flow into the test section (i.e., $Y_c'(0) = Y_c'(1) = 0$).
3. Similarly, the curvature at the inlet and outlet should be zero to promote uniform straight flow (i.e., $Y_c''(0) = Y_c''(1) = 0$).

The non-dimensional 5th order polynomial that satisfies these boundary conditions is $Y_C = (6X_C^5 - 15X_C^4 + 10X_c^3)$.

While, in general, the desired contraction ratio should be maximized, Purdy and Straub (1948) found that a contraction ratio of 9:1 provides a good design compromise between turbulence intensity suppression at a given flow speed and economic constraints. A test section with a square cross section and an area of 36 in^2 combined with a contraction ratio of 9:1 results in a contraction inlet diameter of 20.3-inch. However, for manufacturability purposes, a 20-inch ANSI Class 150 pipe was used for the settling chamber, with an inner diameter of 19.5 inch. The contraction section mates with the settling chamber, and thus should match the inner diameter.

This resulted in a final contraction ratio of 8.5:1 and a cross sectional change from a circular inlet to a square outlet.

4.2.2 Length

The above analysis only provides the desired shape, but not the overall length. The contraction length was selected from existing water tunnel facilities with their contraction lengths scaled with the inlet diameter. A longer contraction section has the potential of introducing a longer boundary layer into the test section. This reduces the amount of test section cross sectional area that has a uniform flow velocity profile. A shorter contraction section has the potential of not providing low enough turbulence intensity in the test section by creating an abrupt cross sectional change that could even lead to flow separation. Table 6 provides the nominal values of *L*/*D* (the length of the contraction section divided by the inlet diameter) for existing low-turbulence water tunnels. The values in Table 6 are based on schematics and photographs of the facilities. For this design, a final L/D value of 1.45 was chosen, which translated to a 29 in. contraction length. This value is consistent with other existing water tunnel designs.

Table 6: Typical L/D ratios for contraction section.

Facilities	**L/D**
LCC	1.24
UNH HiCaT	1.50
Mini LCC	1.65
University of Michigan 9-inch Water Tunnel	0.77
Penn State GTWT	1.69
Penn State 12 inch Water Tunnel	1.55
St. Anthony Falls Water Tunnel	1.67
Average	**1.44**

4.2.3 Thickness

Based on an operating pressure of 40 psi, an initial estimate for the thickness (0.375 inches) was provided by the composites vendor. An FEA analysis using commercial software (SolidWorks Simulation, Dassault Systèmes) was utilized to assess the structural integrity of the contraction section. Fiberglass material properties were obtained from an online materials information database (www.matweb.com accessed on July 2, 2014) and incorporated in the FEA software. A uniform gauge pressure of 40-psi was applied to the inner faces of the contraction section. The two flange surfaces were held stationery. The simulation results are tabulated in Table 7. The results from the simulation denote a factor of safety of 7.7. This factor of safety value was deemed high enough for operational purposes. The supplier of the contraction and diffuser (Diehl Aero-nautical) was given a minimum thickness of 0.375 inch and a maximum of 0.5 inches.

Table 7: FEA Simulation Results for the Contraction Section

Thickness (in.)	0.375
Yield Strength (MPa)	206.84
Max. Von Mises Stress (MPa)	26.84
Max. Displacement (nm)	107000
Max. Strain (με)	184
Factor of Safety	7.7

CHAPTER V

PUMP AND MOTOR SIZING

This section describes the steps taken to size the pump and motor configuration. The main purpose of this water tunnel is to conduct high-speed experiments on Newtonian fluids to study boundary layers. The size of the test section and the test speed required a relatively large volumetric flux of water at a very steady rate in order to study these boundary layers. This limited the pump types to an axial or a centrifugal pump. Based on availability and economic constraints, a centrifugal pump was chosen.

5.1 Pump Flow Capacity Sizing

The required pump capacity was fixed based on the test section geometry (cross sectional area) and the resulting test section speed needed to achieve Re_θ in excess of 10^4. For a given speed and cross sectional area, the volumetric flow rate is equal to the product of the average velocity and the cross sectional area. Even though the required test speed to achieve Re_θ in excess of 10^4 is 10 m/s, 12 m/s was used in the pump capacity sizing to ensure that a conservative estimate was produced. For a 6-inch square test section with an average flow speed of 12 m/s, the flow rate required is 4417 gpm (0.2787 m^3/s). For quoting purposes, pump capacity was rounded up to a flow capacity of 4500 gpm.

Another performance parameter that was taken into consideration for the pump selection was the minimum flow speed capability of the pump. While the primary objective was to achieve a high-Reynolds number flow, the versatility of the water tunnel is dependent on the range of Reynolds numbers it can achieve. As a result, a pump with a lower minimum flow speed is preferred.

5.2 Pump Pressure Head Requirement

A pump's primary purpose is to produce a pressure differential sufficient to drive the flow through the flow loop. This section delineates the approach taken to obtain an accurate pressure head loss estimate for the water tunnel loop. This pressure head loss estimate fed directly to the pump design. The total pressure head loss estimates were heavily dependent on the design of the return leg that is comprised of diffusing pipe sections, straight pipe sections and four short 90° elbows. As a result, it was important to first finalize the return leg design in order to get an estimate of the pressure head requirement. The next sub-section describes the design routine undertaken for the various components of the return leg. The elbows are numbered in clockwise direction starting from the top left corner.

5.2.1 Diffuser Section

The primary purpose of a diffuser section is to reduce the flow speed and thereby, regain pressure in the system. This is achieved by uniform and smooth expansion of the cross sectional area. As noted by Purdy and Straub (1948) and Nedyalkov (2012), a half-angle below 4° provides a good design criterion for a diffuser section. It expands the flow without the risk of flow

separation, which would produce unsteadiness in the loop that will eventually propagate back to the test section.

This flow loop has three diffuser sections. The first diffuser section is made out of fiberglass and is immediately downstream of the test section. This section allows the diffusion of the flow stream before it is directed 90° downward at the Elbow 2 location. The second section is upstream of the pump inlet. This section is comprised of a stainless steel (SS 304) rolled cone with a nominal small diameter of 12 inches and a nominal large diameter of 14 inches. The third section is immediately downstream of the pump outlet and is comprised of a stainless steel (SS 304) rolled cone with a nominal small diameter of 10 inches and a nominal large diameter of 20 inches.

5.2.1.1 Composite Diffuser Section

The diffuser inlet has a square cross section, to match the test section contour. An effective diameter for the diffuser's inlet square section was obtained by equating the area of the square cross section to a circle using the following equation.

$$r_{eq} = a/\sqrt{\pi}$$

Equation 34

Here r_{eq} is the effective radius and a is the side of the square cross section. For a 6-inch square cross section, the effective diameter is 6.77 inches. Following the work of Nedyalkov (2012), the half-angle for the diffuser section can be calculated as

$$\phi = \tan^{-1}\left(\frac{D - 2 * r_{eq}}{2L_D}\right),$$

Equation 35

where D is the diameter of the piping section downstream of the diffuser section and L_D is the length of the diffuser. The diameter of the diffuser outlet section was decided by the diameter of the pipe used for the down leg, which was chosen to be 10 inches. This was based on the availability of steel pipes available, pressure drop in straight pipe sections and the pump inlet diameter. For the given inlet and outlet diameters, a length of 30 inch provided a 3.0° half-angle, which is within the acceptable range to prevent flow separation.

The thickness value of the diffuser section was based on the FEA results. The thickness of the contraction and diffuser were both kept at 3/8 inch. This thickness provided a high factor of safety of 8.9, which was deemed to be high enough for operability. Using the same thickness for contraction and diffuser section also contributed towards ease of manufacturing since both the components were manufactured at the same composites fabrication shop. The results from the FEA simulations are shown in Table 8.

Table 8: FEA simulation results for the fiberglass diffuser section located immediately downstream of the test section.

Thickness	0.375
Yield Strength (MPa)	206.84
Max. Von Mises Stress (MPa)	23.31
Max. Displacement (nm)	55110
Max. Strain (με)	150
Factor of Safety	8.9

5.2.1.2 Rolled Cone Sections

The lower leg of the flow loop is comprised of three rolled cones. A 10-inch by 14-inch rolled cone welded to a 14-inch by 12-inch cone, which is connected to the pump inlet. The contraction from 14-inch diameter to 12-inch diameter before the pump inlet provides uniform

water flow into the pump inlet without the risk of flow separation at different pressure settings. The 10-inch by 14-inch rolled cone has a half-angle of 1.6°. This is much lower than the allowable 4° half-angle (Nedyalkov, 2012; Purdy and Straub, 1951).

Downstream of the pump, the 10-inch by 20-inch rolled cone pipe section diffuses the outlet flow from the pump. The rolled cone is placed at the lower leg in order to avoid sudden geometry changes near Elbow 1, which might lead to flow separation. The half-angle of the 10-inch by 20-inch rolled cone section is 2.9°.

5.2.2 Straight Piping Sections and Elbows

A straight 10-inch pipe section serves as the down leg and connects Elbow 2 and 3. This section is 44 inches in length. The up leg connecting Elbow 1 and 4 is a straight 20-inch pipe that is 18 inches long. The vertical centerline to centerline dimensions for the flow loop is 60 inches. Elbow 1 and 4 are 20 inches in diameter, whereas Elbow 2 and 3 are 10 inches in diameter. Elbow 2 has ANSI flanges to allow the assembly of the flow loop to the diffuser section. Elbows 3 and 4 have ANSI flanges welded to them, in order to aid in assembly. The support structure that holds the flow loop in place is discussed in the next chapter.

5.3 Pressure Head Loss Estimates

Once the design of the flow loop was finalized, pressure head loss estimates could be made for the complete water tunnel loop. Table 9 lists the pressure loss estimates for the various components of the water tunnel.

Table 9: Pressure head-loss estimates for each component of the water tunnel flow loop including the estimated flow conditions.

Component	Qty	K_L	U (m/s)	Δp (kPa)	h_L (m)	h_L (ft)
20-in Elbows	2	0.300	1.4	0.57	0.058	0.19
10-in Elbows	2	0.300	5.5	9.08	0.925	3.04
10 in.Straight Pipe	1	0.081	5.5	1.23	0.125	0.41
20 in.Straight Pipe	1	0.018	1.4	0.02	0.002	0.01
Test Section	1	0.053	12.0	3.84	0.391	1.28
Contraction	1	0.482	12.0	34.73	3.540	11.61
Diffuser	1	0.126	12.0	9.09	0.927	3.04
Honeycombs (HC1, HC2)	1	1.900	1.4	1.80	0.183	0.60
Globe valve	1	4.100	3.8	29.91	3.049	10.00
Bell valve	1	0.040	3.8	0.29	0.030	0.10
10 x 14 Cone	1	0.009	5.5	0.13	0.013	0.04
10 x 20 Cone	1	0.043	5.5	0.02	0.002	0.01
12 x 14 Cone	1	0.003	3.8	0.65	0.066	0.22
Total				**91**	**9.3**	**30**
Motor Power Required				**46.3 hp**		
Factor of Safety				**3.2**		

As seen in Table 9, K_L is defined as the non-dimensional pressure loss coefficient, U is defined as the flow speed, Δp is defined as the pressure loss and h_L is defined as the pressure head-loss (expressed in m or ft). Based on the K_L values, Δp and h_L were calculated using

$$\Delta p = K_L \left(\frac{\rho U^2}{2}\right) \text{ and}$$

Equation 36

$$h_L = K_L \frac{U^2}{2g},$$

Equation 37

where g is the acceleration due to gravity (9.81 m/s^2). The pressure loss coefficients (K_L) for the piping components were obtained from the Moody Chart for pipe flow (White, 2006) and commercial data compiled for gradually expanding and contracting pipe sections, pipe fittings

and valves (Heald, 2010). Pressure loss coefficient for the honeycomb section was based on the honeycomb sizing charts provided by Lumley and McMahon (1967).

Typically estimated head losses following the above approach are biased low, which suggests that a relatively large factor of safety should be applied to the estimate. For quoting purposes, a 100 ft. of pressure head was utilized. This is expected to be sufficient to ensure that the pump and motor combination would be able to overcome unaccounted pressure head losses (due to swirl and non-uniformity in the flow) once the final configuration is fabricated and installed. Moreover, the extra pressure head can also be used for additional flow conditioning, in case the test section flow quality is not as predicted. This led to a factor of safety of 3.2.

5.3.1 Motor Sizing

Given the required 4500 gpm flow rate and 100 ft of pressure head, the final choice for the pump was a horizontal split casing 12×10×12 centrifugal pump (S10B12A-4, Patterson). This specific pump was selected amongst seven possibilities because (1) it had one of the lowest minimum flow rates, (2) lowest cost and (3) its size did not impact the design of the rest of the tunnel. The performance curve for this pump is shown in Figure **16**, which shows that in order to achieve a 4500 gpm flow rate with a pressure head of 100 ft, a 150 hp motor is required. This resulting motor requirement shown in Figure **16** is consistent with the motor power calculations that were based on the pressure loss estimates, as given in Table 9.

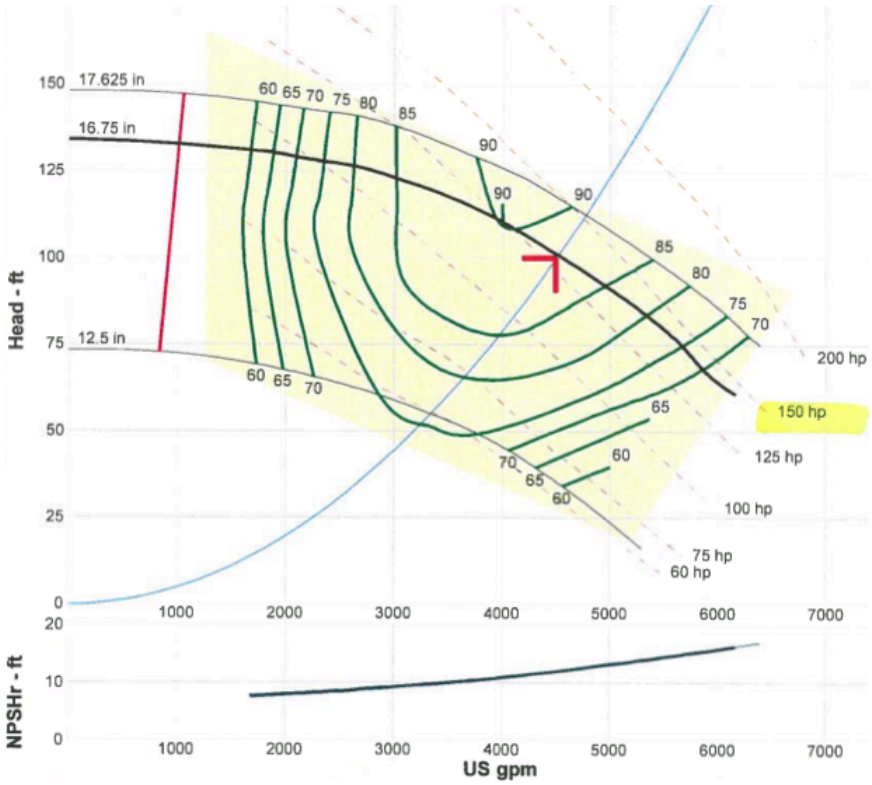

Figure 16**: Pump performance curve for the centrifugal pump selected for the water tunnel (S10B12A-4, Patterson).**

CHAPTER VI

DESIGN OF SUPPORT STRUCTURE AND INSTALLATION PROCEDURES

This section highlights the installation procedures that will be used to install the water tunnel in the High Reynolds Number Fluid Mechanics Laboratory at Oklahoma State University. A description of the support structure is also provided in this section. The right side view of the water tunnel loop along with the labeled individual components, as shown in Figure 17, will be used as a reference for individual component numbers in this chapter. The numbering starts from the top left with the 20-inch 90° short radius elbow and increases in the clockwise directions.

Part Number	Description	Part Number	Description
1	Elbow 1	9	Down Leg Piping
2	Honeycomb (HC1)	10	Elbow 3
3	Settling Chamber and Honeycomb (HC2)	11	10" X 12" Rolled Cone
4	Contraction	12	Pump Inlet Piping
5	Test Section	13	Pump and Motor
6	Diffuser	14	10' X 20" Rolled Cone
7	Straight Pipe	15	Elbow 4
8	Elbow 2	16	Up Leg

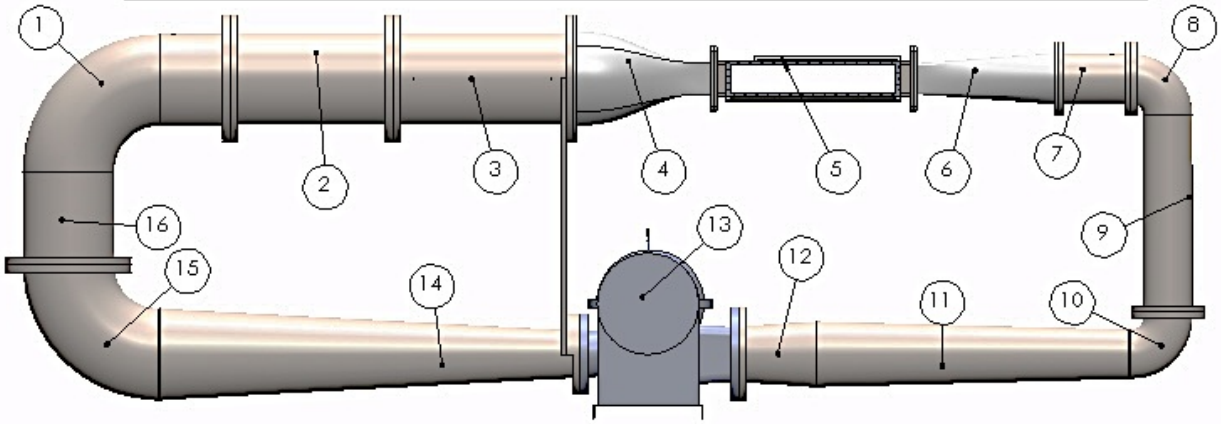

Figure 17: Side view of the water tunnel flow loop. Individual parts/components are numbered with their description provided in the table above the schematic.

6.1 Total Volume and Weight Estimates

In order to size the support structure for the water tunnel flow loop, a weight and volume estimate of the complete loop was required. This estimate was based on known weight estimates of standard stainless steel piping sections and flanges (Heald, 2010), and weight and volume estimates of composite parts from Solidworks. The weight of each component in the flow loop along with the water weight and volume is given in Table 10.

Table 10: Weight and Volume of Individual Components

Part	Weight (lb.)	Volume (in^3)	Water Weight (lb.)	Total Weight (lb.)
Settling Chamber	551	10722	386	937
10" x 20" Rolled Cone	359	14970	539	898
Honeycomb Sections	547	7353	265	801
20-inch Piping	357	10906	393	749
Elbow 4	291	9367	337	628
10" x 14" Rolled Cone	238	10732	386	624
Elbow 1	94	9367	337	431
Test Section	239	1512	54	293
10-inch Piping	130	4224	152	282
Contraction	76	4457	160	236
12" x 14" Rolled Cone	137	2261	81	219
Diffuser Transition Piece	133	1408	51	184
Elbow 2	78	1238	45	123
Elbow 3	78	1238	45	123
Diffuser	49	1773	64	113
Pump and Motor	1500			
Transformer	1500			
Support Structure	2500			
TOTAL	**8855**	Without Water		
	12150	With Water		

Table 10 shows that the weight of the water in the loop is a considerable amount (~3300 lb.). The settling chamber is the heaviest component in the flow loop. The second heaviest component in the flow loop is the 10-inch by 20-inch rolled cone. The same component also has the highest volume contribution. The composite built diffuser section is the lightest component in the flow loop.

6.2 Design of Support Structure

The water tunnel flow loop will be supported such that the load path from the water tunnel flow loop terminates in the building structure (i.e., the support structure will be rigidly

attached to either the ceiling or the floor). Figure 18 below shows the support structure and the assembled water tunnel.

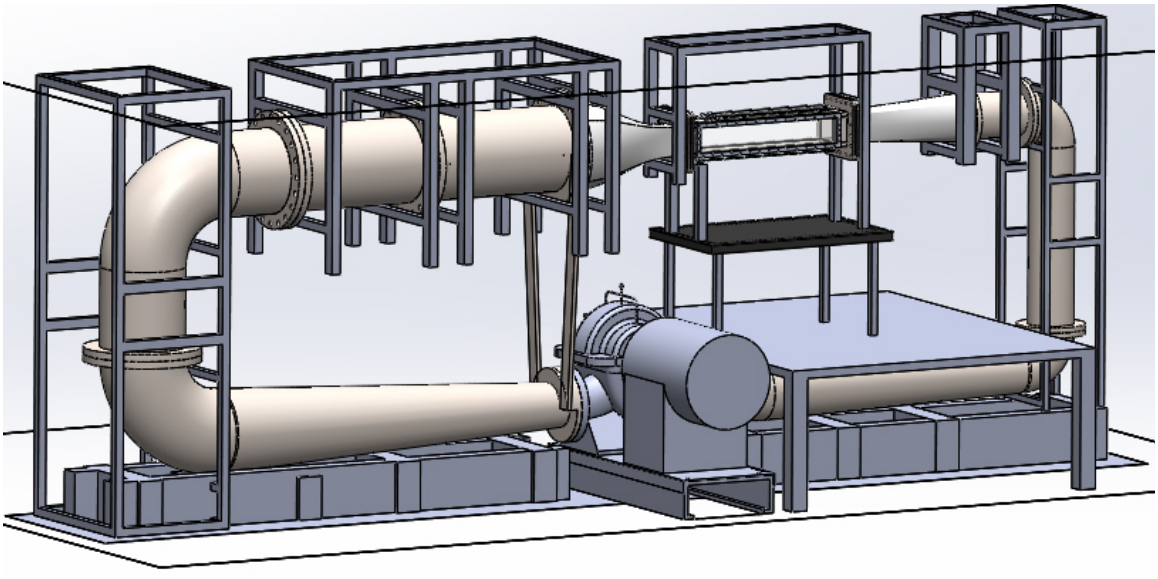

Figure 18: Schematic of the assembled water tunnel including the proposed support structure.

The complete water tunnel will be assembled on top of a quarter inch stainless steel plate. This will ensure sufficient load distribution in order to achieve a floor loading of less than 150 lb./ft^2. In order to allow the pump and motor to be shared with the multi-phase flow loop, the pump and motor configuration should be movable. As a result, the support structures for the lower leg were of crucial importance. Two C-channels (C 9X15) will be placed underneath the pump and motor assembly and bolted to the floor. The C-channels will allow the transfer of the loads to the floor. Two bolt patterns will be created on the C-channel to allow the movement of pump and motor configuration for the multi-phase flow experiments using a pallet jack. The two rolled cones will be supported using two (W 12 X 65) I-beams each, which run the length of the rolled cone, and eight cross sectional I-beams. The T-beams will connect the rolled cones to the I-

beams, which will be bolted to the floor. This creates a load path from the rolled cones to the lab floor.

Unistrut sections will be bolted to the floor and the ceiling of the laboratory. These sections will allow the assembly of vertical unistruts that will act as support structure. The straight piping section on the top leg will be supported using 1-5/8" unistruts. Four unistruts will be bolted to two points on the pipe, two on top and two on bottom, thereby keeping it fixed in all three dimensions. This design should also dampen out the vibrations since the unistruts will be connected directly to the building via the ceiling or the floor. Eight 1-5/8" unistruts will span the laboratory room height (four at both ends) and will be connected to the up and down leg of the flow loop as shown in Figure 18. These unistruts will be connected to the straight 10-inch and 20-inch piping section and the four elbows.

Two angled metal beams will also connect the settling chamber to the rolled cone flange (on the pump outlet side). This will assure that the piping section is rigidly supported, in case the contraction needs to be removed from the loop. Without these metal bars, there is a chance that the complete load of the top leg will be resting on the flange face of Part 16, if the contraction section is not in place.

An optical table will be placed 1.5 ft. directly underneath the test section. The optical table will be supported by unistruts and the platform that will be placed underneath the optical table. The height of the platform is 4.5" from the test section. This height allows easy access to the test section. This platform will be held using four unistruts that are bolted to the unistrut track on the floor. This secures the test section, optical table and platform to the ceiling and the floor of

the laboratory. This ensures that the optical table and the platform are rigidly supported and a load path is formed from the ceiling to the roof.

6.3 Additional Features of the Flow Loop

This section addresses design features of the flow loop that involves drainage connections, pressure regulation of the water tunnel, pump and motor isolation to dampen vibrations and spill containment techniques that will be utilized for this water tunnel.

6.3.1 Drain

The two low points on the lower leg of the loop will have drainage holes added to facilitate draining and filling of the tunnel. A 3-inch NPT nipple is being added upstream of the pump inlet. This will serves as the primary inlet/outlet port and will be plumbed into both the building cold water line and the drainage system. A 1.5 inch NPT nipple is placed on Elbow 3 to allow drainage of the water that has accumulated downstream of the pump (see drawings in Appendix A for more detail).

6.3.2 Pressure Regulation System

Two ¾ inch NPT nipples are welded to the top leg of the flow loop at each of the high points on Elbows 1 and 4. These outlets will be directly connected to a pressure vessel. This pressure vessel will be connected to a compressed air line. This compressed air line will be controlled using a pressure regulator, which will set the tunnel pressure during operation. The tunnel is designed for a maximum pressure loading of 40 psi. The pressure vessel will also be used for the removal of air bubbles, before testing. Two additional ports holes are included in the

settling chamber to allow pressure and temperature measurements via pressure probes and thermocouples. Details on the location and diameter of these port holes and outlets can be found in Appendix A.

6.3.3 Pump Isolation System

The pump and motor section will be isolated from the water tunnel flow loop in order to reduce the vibration in the flow loop and velocity fluctuation levels in the test section. The discharge and suction faces of the pump will be connected to elastomer flex joints in order to absorb vibrations from the pump and motor configuration.

6.3.4 Spill Containment System

A spill berm will be used to contain any spills from the water tunnel. The spill berm will outline the water tunnel and the support structure and also contain the main drain outlet in the laboratory room. The spill berm will be 2.25” high and the straight berm sections will be connected using corner connections to form a rectangular outline outside the assembled water tunnel.

6.4 Installation Procedure

This section delineates the process that will be undertaken to assemble the water tunnel. Pallet jacks and a hoist will be used to move the major components in place before it is assembled to the loop.

1. All the major components will be brought into the laboratory from the docking station in the ATRC using pallet jacks through the double doors.
2. Once the 440V line is secured, the pump and the motor will be positioned on the lab floor.
3. Next the hoist will be used to place parts 14 and 15 adjacent to the pump. Once in position and connected to the support structure, the 10” flange will be bolted to the pump face.
4. A similar process will allow the assembly of the removable upstream piping section (parts 10, 11 and 12). This completes the assembly of the lower leg.
5. Eight unistruts will be bolted to the floor. These unistruts will be used to install the long unistruts that span the laboratory room height.
6. Four unistruts each will be installed at the two ends of the lower leg. These unistruts will span the lab height. These unistruts will be used to secure the up and down leg (parts 1,8, 9,10,15 and 16). Prior to assembly, the O-rings will be installed on parts 9 and 16. All the parts will then be connected to the unistrut. After the unistrut and O-ring installation, parts 1,8, 9 and 16 will be held in place by bolting the flanges to the existing flange faces on the parts 10 and 15. Unistruts from the ceiling and the floor will be used to anchor the elbows in place. This completes the assembly of the up and down leg.
7. After the assembly of the up and down leg, position of the remaining parts will be marked on the ceiling to allow the installation of the remaining unistruts that will act as the support structure. After the installation of the unistruts, parts 2-7 will be installed one at a time. Each part will be held in place using the hoist. Corresponding unistrut will be connected to each part as described before. Then, each part will be bolted to the corresponding flange face. O-ring will be installed on parts 2,3 and 7 prior to installation.
8. At the junction between the metal and composite parts (Part 3, 4, 6 and 7), an appropriately shaped gasket will be installed prior to assembly, to avoid water leakage.

9. The final part, Part 7, will be installed, once the gap between the parts 6 and 8 is accurately determined. Part 7 will be then fabricated in order to finish the loop without leakage. Both the flanges of Part 7 will have O-rings, in order to avoid leakage. The flange faces will be first bolted to Part 6 and Part 8. Once the mating of both the flange surfaces is deemed satisfactory, Part 7 will be attached to its support structure as well. This finishes the complete water tunnel flow loop assembly.
10. Using an adjustable height crane, the optical table will be moved in place, 1.5 ft below the test section. Once in position, the hoist will be used to hold the test section and to relieve the loads on the flange bolts. Four bolts from the lower row on the test section flange will be removed in order to allow the placement of the support structure that holds the optical table. This will secure the optical table to the test section via the two metal plates being attached to the flanges. These bolts will hold the contraction, test section, unistruts and the metal plates in place.
11. Once the optical table is secured to the test section, the position of the platform will be marked on the floor.
12. Four vertical unistruts will be installed to create a space for the platform. Once the platform is installed, it will be bolted to the unistruts.
13. Four more unistruts will be used to attach the optical table to the platform.
14. The two NPT Nipples on the top leg will be connected to the pressure vessel.
15. The cold water supply will be connected to the 3” water inlet/outlet connection.

CHAPTER VII

SUMMARY AND FUTURE WORK

7.1 Summary

This thesis describes the process that was utilized in the design of a high Reynolds number recirculating water tunnel at Oklahoma State University. The main purpose of this water tunnel is to use state-of-the-art flow imaging diagnostic tools to study high Reynolds number turbulent boundary layers that are modified with active polymers. One of the motivations to study this field is to explore the potential of drag reduction in Naval applications. One of the design constraints was to achieve a momentum thickness based Reynolds number (Re_θ) value of 10^4. This value was based on filling the gap between commercially available water tunnel facilities ($Re_\theta \sim 10^3$) and the world's largest water tunnel facilities($Re_\theta \sim 10^5$).

The test section of this water tunnel was initially sized using theoretical estimates from a flat plate analysis without a pressure gradient. This analysis coupled with a Re_θ requirement of 10^4 and space and economic resource constraints resulted in a 6-in. (0.16 m) square cross section with a test section length of 1 m. The validity of the zero-pressure-gradient assumption was confirmed by estimating the dimensionless acceleration parameter for our boundary layer and showing it was more than two orders of magnitude lower than empirically established values (Patel, 1965). This water tunnel is rated for a test section speed of 10 m/s and a maximum operational pressure of 40 psi. The final design of the test section provides ample optical access

for PIV imaging of the near wall region. The surface roughness finish was selected such that the test section walls can be considered hydraulically smooth ($k^+ < 1$). FEA simulations provided factor of safety estimates for the stainless steel frame and the acrylic plate components, which were 244 and 4, respectively. Bolt spacing and sizing analysis was performed to ensure a high factor of safety (85) for the bolts that will hold the test section components together (Tessco Technologies, 2014). O-Ring sizing (Parker Handbook, 2007) was also performed to ensure optimal face sealing and to avoid water leakage.

The flow conditioning in this water tunnel is comprised of two honeycomb sections, a settling chamber and a contraction section. The honeycomb section is composed of a pair of honeycombs. The first section (HC1) has a hexagonal cell size of 0.75 in and length of 24 in, and the second (HC2) has a cell size of 0.25 in and length of 6 in. These sizes were selected based on sizing charts (Lumley and McMahon, 1967). The advantage of the second stage of honeycombs was illustrated by showing for an incoming turbulence intensity of 13%, the test section turbulence intensity is reduced from 0.7% to 0.2%. A 29-inch long settling chamber follows the honeycomb, which is used to dissipate the turbulence generated from the honeycombs. The contraction profile shape is a 5^{th} order polynomial curve, as recommended by the experimental results from Bell and Mehta (1988). The contraction area ratio is 8.5:1, which is slightly below the recommended 9:1 ratio (Purdy and Straub, 1948) due to a desire to use standard pipe sizes. The contraction length of 29 in. was chosen based on an average length to diameter ratio of 1.44, as determined from other predominant water tunnels around the world. The contraction section was manufactured using composites material. Fiberglass was chosen because of the cheaper manufacturing cost and its molding capabilities to accommodate complex cross sectional shape change (from a circular inlet to a square outlet). Based on manufacturer recommendations and FEA simulations, 3/8 inch was specified as the minimum thickness for the contraction.

Three diffuser sections are used within the water tunnel loop. The half-angle of all the diffusers were kept under 4° to prevent flow separation (Purdy and Straub, 1948; Nedyalkov 2012). The first diffuser section is made out of fiberglass and is placed immediately downstream of the test section. It expands the flow from a 6-in. square cross section to a 10 in. circular cross section over a 30 in. length, which results in a 3° half angle The thickness of the diffuser section is kept at 3/8 in. as well to aid manufacturing, which gives a factor of safety of 8.9. The remaining two diffuser sections, made out of stainless steel (SS 304) rolled cones, are placed upstream and downstream of the pump section. The upstream diffuser section expands the flow from a 10 in. circular cross section to a 14 in circular cross section, resulting in a half angle of 1.6°. The downstream diffuser section expands the flow from a 10 in. circular cross section (the pump outlet) to a 20 in circular cross section. This resulted in a half angle of 2.9°. In effect, the three diffuser sections expand the flow from a 6-inch square cross section (test section) to a 20-in circular cross section without the risk of flow separation.

The high volumetric flux and steady rate requirements needed to study the turbulent boundary layers limited the pump types to axial and centrifugal pumps. Test section sizing resulted in a pump capacity requirement of 4500 GPM. Pressure head loss estimates (30 ft.) for all the components in the water tunnel flow loop provided a power requirement of 49 hp. The final motor selection was upsized to 150 hp (pressure head of 100 ft.) in order to accommodate unaccounted pressure head losses due to non-uniformity and swirl in the flow. This provided a factor of safety of 3.2. The excess pressure head can also be used for additional flow conditioning, if deemed necessary. The final pump selection was a Patterson Horizontal Split Casing 12x10x12 Centrifugal Pump.

The pump and motor configuration is designed to be movable in order to allow the sharing of the pump and motor with the multi-phase flow loop facility. All the straight piping sections are held in place using unistrut support structure. Eight unistrut structures span the laboratory height and create a load path from the water tunnel flow loop to the building structure. This ensures that the vibrations are dampened out and the flow loop is rigidly supported. The diffuser sections upstream and downstream of the pump are supported by I-beams and cross sectional T-beam supports. Two angled metal beams also connect the settling chamber to the diffuser section downstream of the pump. This ensures a rigid support structure for the top leg of the flow loop when the contraction section is removed. An optical table and a platform are placed below the test section for operational access. The platform is supported using four unistruts that are bolted to the floor. The optical table is supported using the vertical unistruts from the ceiling and the platform. Two ¾-inch NPT nipples are welded to the top leg of the flow loop. These outlets will be connected to a pressure vessel. This pressure vessel will allow the removal of air bubbles and control of the pressure conditions inside the water tunnel loop. A drainage outlet and a water inlet section are also welded to the bottom leg of the flow loop.

The final flow loop is comprised of four 90° short radius elbows, 10 in. and 20 in. straight piping sections, three diffuser sections, two honeycomb units, a 8.5:1 contraction section, a high optical access test section and a pump and motor configuration with a factor of safety of 3.2.

7.2 Future Work

Currently, the test section, the contraction and the diffuser sections are being fabricated. The pump and motor has been purchased. The piping section has been sent out for bid.

Fabrication of these pieces will begin in the near future. The honeycomb sections will be purchased after the piping section bid is finalized. The following list delineates the recommended future work in order to make this water tunnel operational.

1. Complete fabrication of the piping section.
2. Obtain all the components and move them to the Laboratory using pellets jacks form the ATRC docking station.
3. Finalize the details of the support structure design.
4. Assemble the water tunnel and the support structure.
5. Secure a 440 V power line for the pump and motor setup.
6. Connect the water tunnel flow outlet to the building's cold water line and the drainage system.
7. Set up the high power laser system and the optical system to perform speed calibration and flow quality tests.
8. Modify flow-conditioning unit (if needed, to reduce turbulence level).
9. Calibrate the pressure regulator that is connected to the pressure vessel to operational pressure level in the water tunnel.
10. Calibrate the pump and motor drive to the test section speed.
11. Characterize the test section flow.

BIBLIOGRAPHY

AISC 2005 Bolt Spacing Standards *AISC* **J3.2 P1.6 – 106**.

ARNDT, E.A.R. AND WEITENDORF, E.A. 1990 Hydrodynamic considerations in the design of the hydrodynamics and cavitation tunnel (HYKAT) of HSVA *Technical Paper* **283 Series A**, St. Anthony Falls Laboratory

ARNDT, R. E. A., ARAKERI, V. H., AND HIGUCHI, H. 1991 Some Observations of Tip Vortex Cavitation *J. Fluid Mech*., **229**, pp. 269–289

BATCHELOR, G.K. 1960 The Theory of Homogeneous Turbulence, *The University Press,* Cambridge, England.

BELL, J.H AND MEHTA, R. D. 1988 Contraction design for small low-speed wind tunnels *NASA STI/Recon* Technical Report **N, 89:13753**

DEUTSCH, S & CASTANO, J 1986 Microbubble skin friction reduction on an axisymmetric body *Physics of Fluids*, **29**(11), 3590-3597.

ETTER, R.J., CUTBIRTH, J. M., CECCIO, S.L., DOWLING, D.R., AND PERLIN, M. 2005 High Reynolds number experimentation in the US Navy's William B Morgan Large Cavitation Channel, *Meas. Sci. Technol.* **16** 1701–1709

FONTAINE, AA & DEUTSCH, S 1992 The influence of the type of gas on the reduction of skin friction drag by microbubble injection *Experiments in Fluids*, **13**, 128-136.

G. F. OWEIS, J. CHOI, AND S. L. CECCIO 2004 Dynamics and noise emission of laser induced cavitation bubbles in a vortical flow field *J. Acoust. Soc.* Am.**115, 1049**

GINDROZ, B. & BILLET, M.L. 1998 Influence of the nuclei on the cavitation inception for different types of cavitation on ship propellers *Journal of Fluids Engineering*, **120**(1), 171-178.

HEALD, C.C. 2010 Cameron Hydraulic Data 19th Edition *Cameron Hydraulic Data*

JERZ, R. 2014 Retrieved from *http://user.engineering.uiowa.edu/~mie032/lectures /17surface_roughness_and_machining_symbols_full.pdf*

LAUCHLE, G.C. & GURNEY, G.B. 1984 Laminar boundary-layer transition on a heated underwater body *Journal of Fluid Mechanics*, **144**, 79-101.

LEHMAN, 1959 ARL Penn State Report No. NORD 16597-56, Fluid Dynamics Department, Applied Research Laboratory, The Pennsylvania State University

LEROUX, J.-B., ASTOLFI, J.A. & BILLARD, J.Y. 2004 An experimental study of unsteady partial cavitation, *Journal of Fluids Engineering*, **126**, 94-101.

LOEHRKE, R. J. AND NAGIB, H. M. 1976 Control of Free- Stream Turbulence by means of Honeycombs – A Balance Between Suppression and Generation *ASME Journal of Fluids Engineering*, Vol. **98**, pp. 342-355.

LUMLEY, J.L. AND McMAHON, J.F. 1967 Reducing Water Tunnel Turbulence by Means of a Honeycomb *ASME Journal of Basic Engineering,* Vol. **89**, Dec. pp. **764-770**

MADAVAN, NK, DEUTSCH, S &MERKLE, CL 1984Reduction of turbulent skin friction by microbubbles *Physics of Fluids*, **27**, 356.

MAKIHARJU, S.A., ELBING, B.R., WIGGINS, A., SCHINASI, S., VANDEN BROECK, J.-M., PERLIN, M., DOWLING, D.R. & CECCIO, S.L. 2013 On the scaling of air entrainment from a ventilated partial cavity *Journal of Fluid Mechanics*, **732**, 47-76.

MARBOE, R. C., et. al., 1993 Hydroacoustic Research capabilities in the Large Water Tunnel at ARL-Penn State *Proceedings of Symposium on Flow Noise Modeling, Measurement, and Control*, NCA-VOL **15**/FED-VOL **168**, pp. 125-135, ASME Winter Annual Meeting

MATWEB 2014 Retrieved from: *http://www.matweb.com/search/datasheet.aspx?matguid =3f2253a553404b13893830617250b5d8*

MORI, T., KOMATSU, Y., KANEKO, HIROBUMI, SATO, R., IZUMI, H., YAKUSHIJI, R. & IYOTA, M. 2003 Hydrodynamic design of the Flow Noise Simulator *Proceedings of the ASME/JSME 2003 4th Joint Fluids Summer Engineering Conference*, FEDSM2003-45304, 135-140, Honolulu, Hawaii.

NEDYALKOV, I. 2012 Design of Contraction, Test Section and Diffuser for a High-Speed Water Tunnel. Retrieved from *Chalmers Publication Library.*

PARKER HANNIFIN CORPORATION 2007 *Parker O-Ring Handbook*, 50th edition.

PATEL, V.C. 1965 Calibration of the Preston tube and limitations on its use in pressure gradients *Journal of Fluid Mechanics* **23,** 185-208.

PURDY, H.D. AND STRAUB, L.G. 1948 Model experiments for the design of a sixty inch water tunnel *Technical Report* **10,11,12,13,14,15**, St. Anthony Falls Hydraulic Laboratory, University of Minnesota

RIPKEN, J. F. 1951 Design Studies for a Closed-Jet Water Tunnel *Technical Report* **9, Series B,** University of Minnesota, St. Anthony Falls Laboratory.

SHEN, X., CECCIO, S.L. & PERLIN, M. 2006 Influence of bubble size on micro-bubble drag reduction *Experiments in Fluids*, **41**, 415-424.

TESSCO TECHNOLOGIES 2014 Bolt Grade Marking and Strength Retrieved from *www.tessco.com/yts/customerservice/techsupport/whitepapers/pdf/bolt_grade.pdf*

WETZEL J.M. AND ARNDT R.E.A. 1994a Hydrodynamic design considerations for hydroacoustic facilities: Part I. Flow quality *ASME J. Fluids Eng*. **116** 324–31

WHITE, F. 2006. Viscous fluid flow. New York, NY: *McGraw-Hill Higher Education.*

WOSNIK, M. AND ARNDT, R. 2006 Testing of a 1:6 scale physical model of the large, low-noise cavitation tunnel (LOCAT). *Technical Report* **486**, St. Anthony Falls Laboratory.

APPENDICES

APPENDIX A

This section contains the technical drawings that were used for the piping section, the test section and the composite parts (contraction and diffuser sections). These final drawings will be used by the machinists to fabricate the individual components and assemble the part.

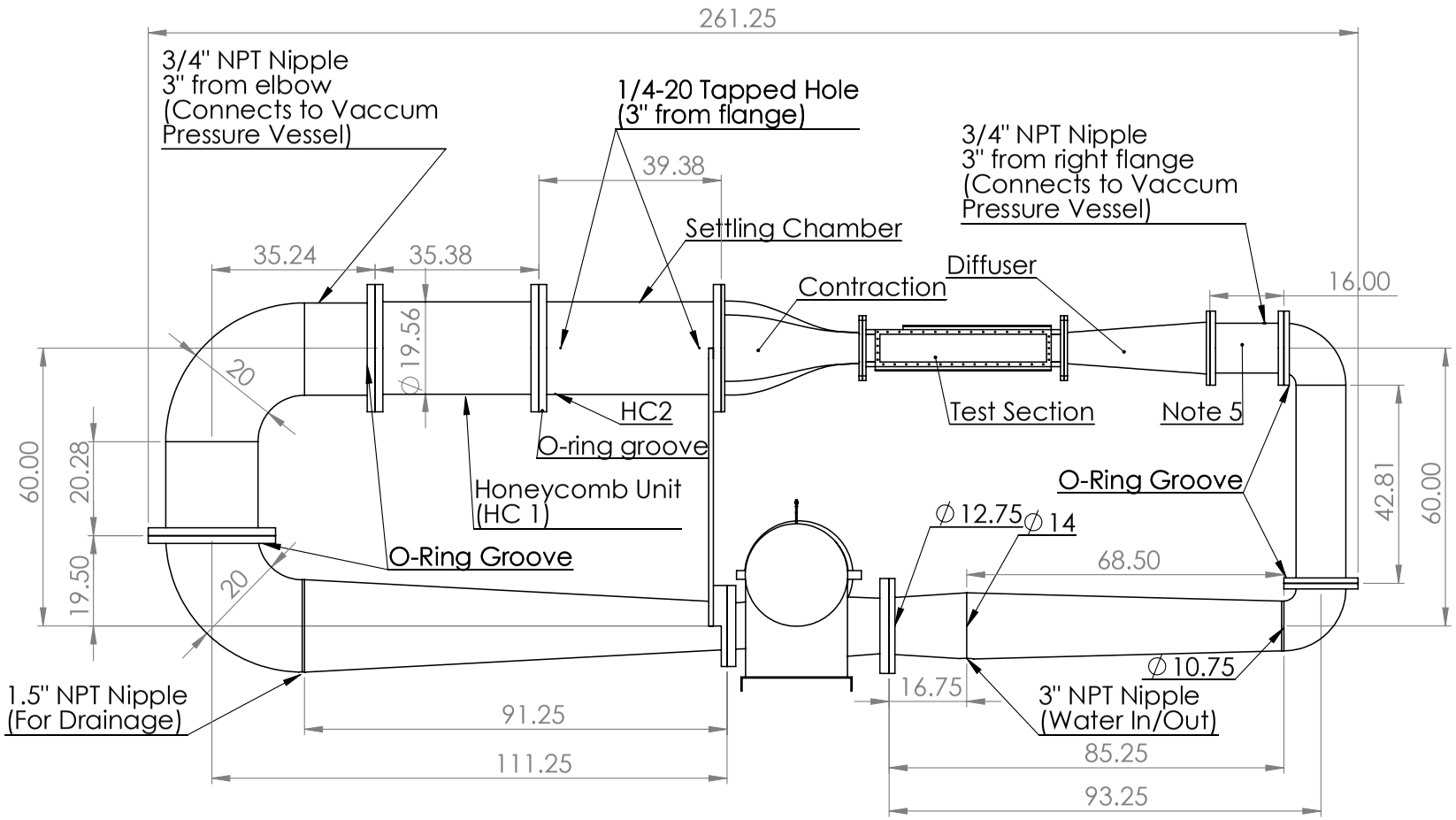

72

Note 1: ANSI 150 Flange 10" (Total: 6)
Note 2: ANSI 150 Flange 12" (Total: 1)
Note 3: ANSI 150 Flange 20" (Total: 7)
Note 4: Five O-Ring grooves

Note 5: Length of this piece is varialbe.
Fabricate once rest is installed to assure the correct length.

Note 6: Honeycomb structure will be welded on non-weld neck portion.
HC1 Length: 24", HC2 Length: 6"
Weld HC1 to Honeycomb Unit
Weld HC2 after left flange of Settling Chamber
Honeycomb Unit Diameter matches 20" Sch 10 Pipe

DECIMAL POINT	TOLERANCE
0.1	±0.08
0.01	±0.04
0.001	±0.005
UNLESS OTHERWISE SPECIFIED	

Rev. No. 07	Date: 07/05/14
Details: Added second Honeycomb Section	

PART NAME	SCALE	MATERIAL	QTY	REV
RETURN LEG	1:30	STAINLESS STEEL	1	-

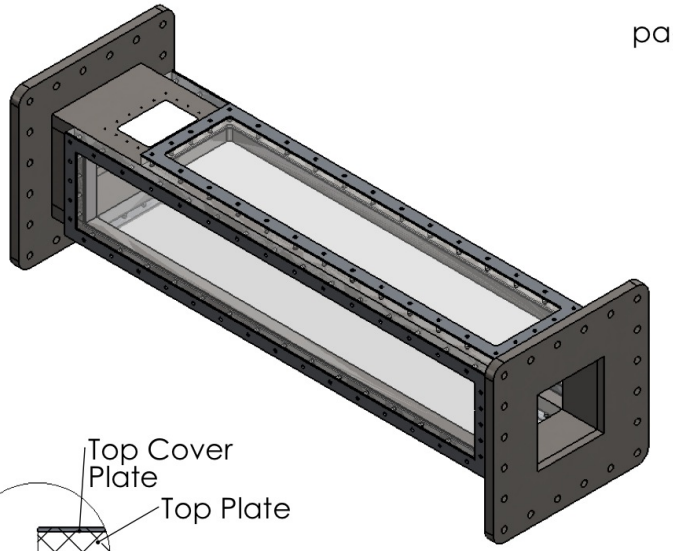

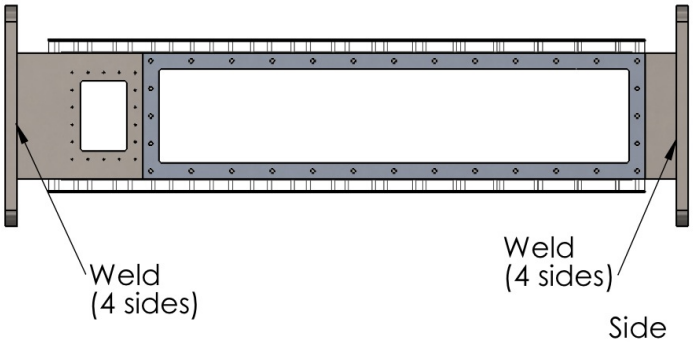

Note: Chamfers will be added to Spreader, Top Frame and Bottom Frange to assist welding to Flange

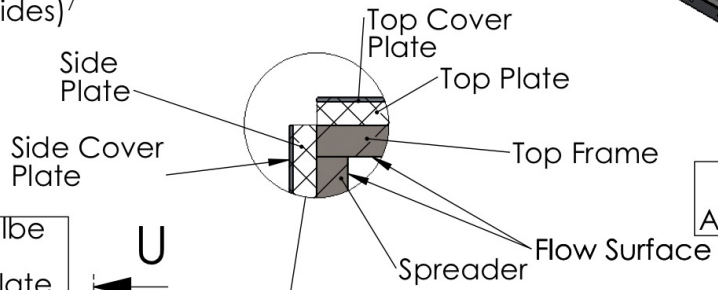

All Flow Surfaces: 32

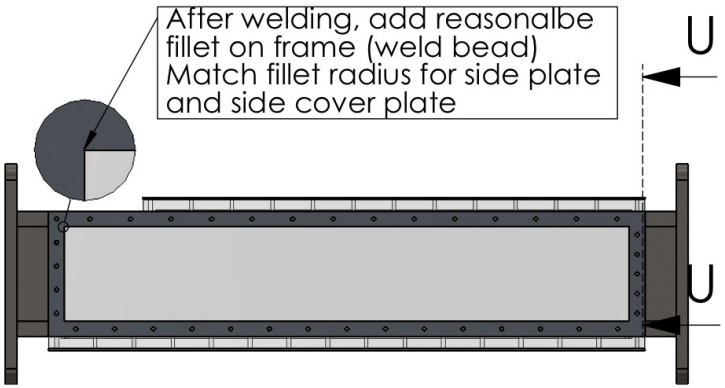

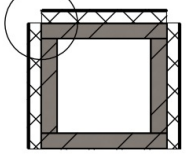

SECTION U-U

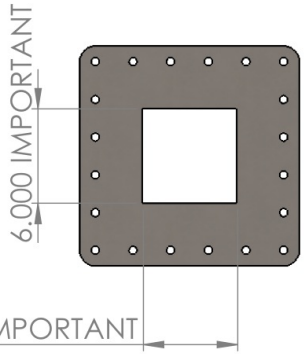

O-RING GROOVES:
IF TOOLING MARKS PRESENT, SHOULD BE LONGITDUINAL

DECIMAL POINT	TOLERANCE
0.1	±0.08
0.01	±0.04
0.001	±0.005
UNLESS OTHERWISE SPECIFIED	

Rev. No. 01	Date: 06/07/14
Details: Updated width and thickness of plates, fillet radius	

PART NAME	SCALE	MATERIAL	QTY	REV
TEST SECTION	1:10	AS SPECIFIED	1	-

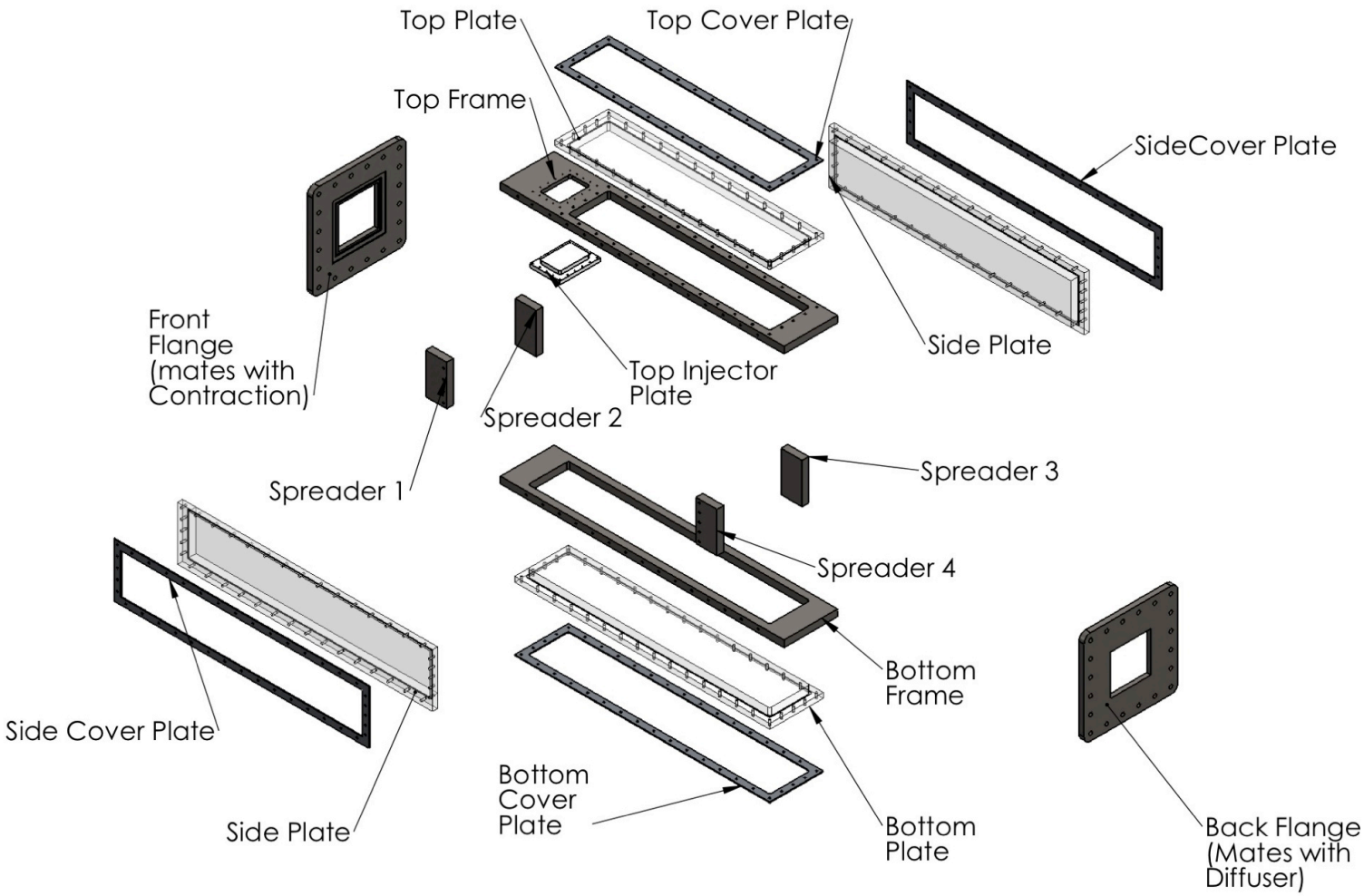

DECIMAL POINT	TOLERANCE
0.1	±0.08
0.01	±0.04
0.001	±0.005
UNLESS OTHERWISE SPECIFIED	

Rev. No. 00	Date:06/07/14
Details:	

Top Frame, Bottom Frame and Spreaders recesses 1/8" into both flanges

PART NAME	SCALE	MATERIAL	QTY	REV
TEST SECTION	1:15	-	1	-

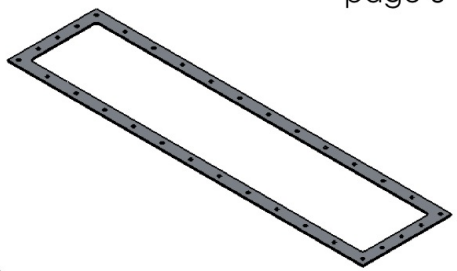

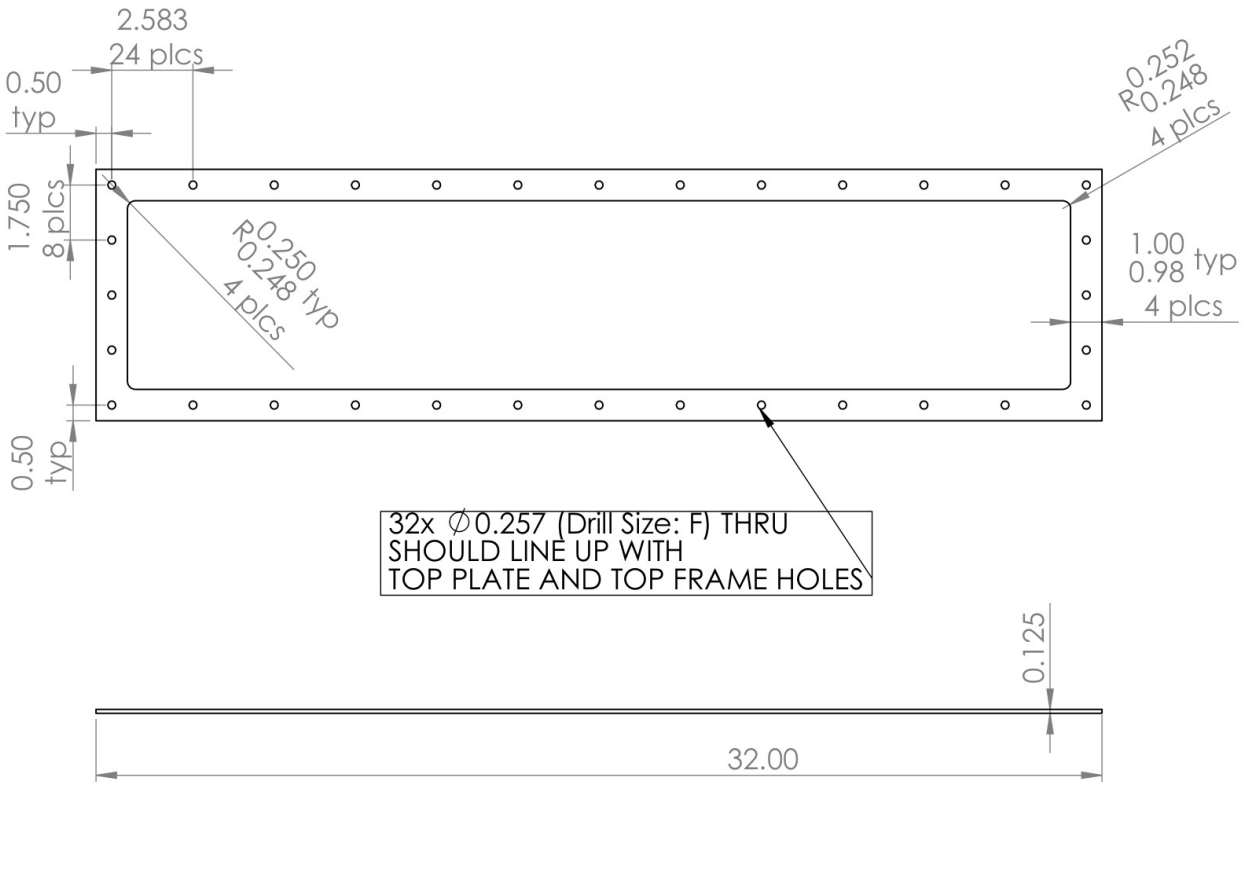

DECIMAL POINT	TOLERANCE
0.1	±0.08
0.01	±0.04
0.001	±0.005
UNLESS OTHERWISE SPECIFIED	

Rev. No. 01	Date:06/07/14
Details: Updated holes, width, fillet radius	

PART NAME	SCALE	MATERIAL	QTY	REV
TOP COVER PLATE	1:5	ALUMINUM	1	-

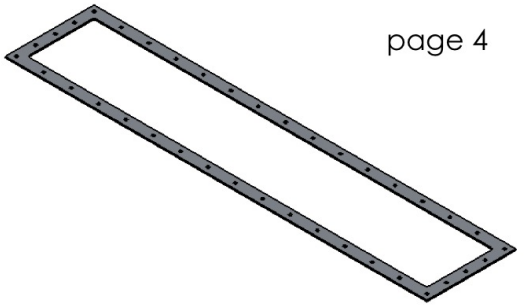

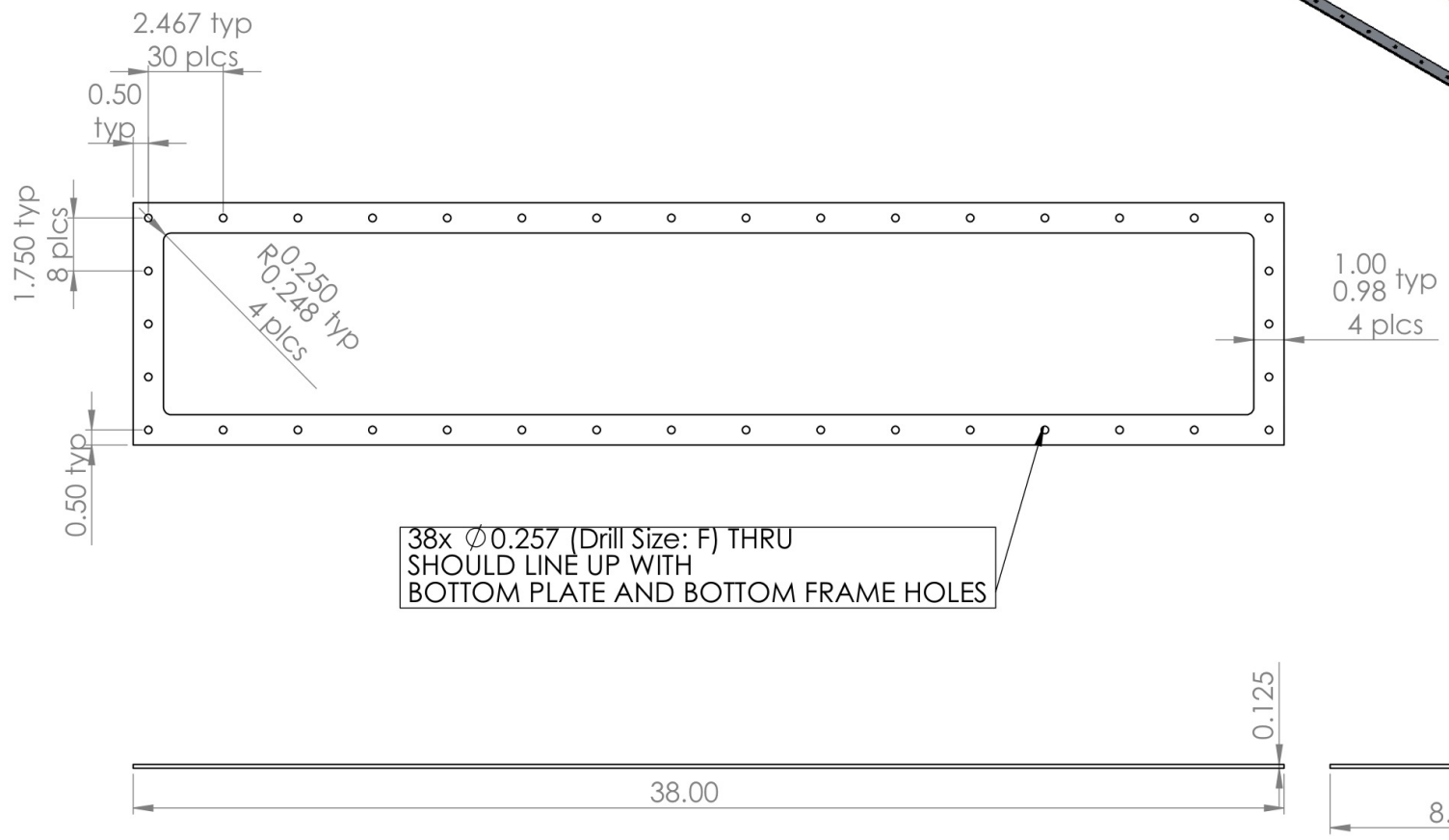

DECIMAL POINT	TOLERANCE
0.1	±0.08
0.01	±0.04
0.001	±0.005
UNLESS OTHERWISE SPECIFIED	

Rev. No. 01	Date: 06/11/14
Details: Updated holes, width, fillet radius	

PART NAME	SCALE	MATERIAL	QTY	REV
BOTTOM COVER PLATE	1:5	ALUMINUM	1	-

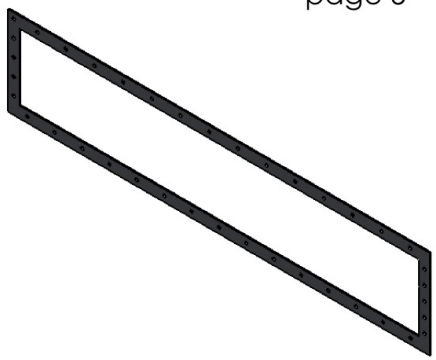

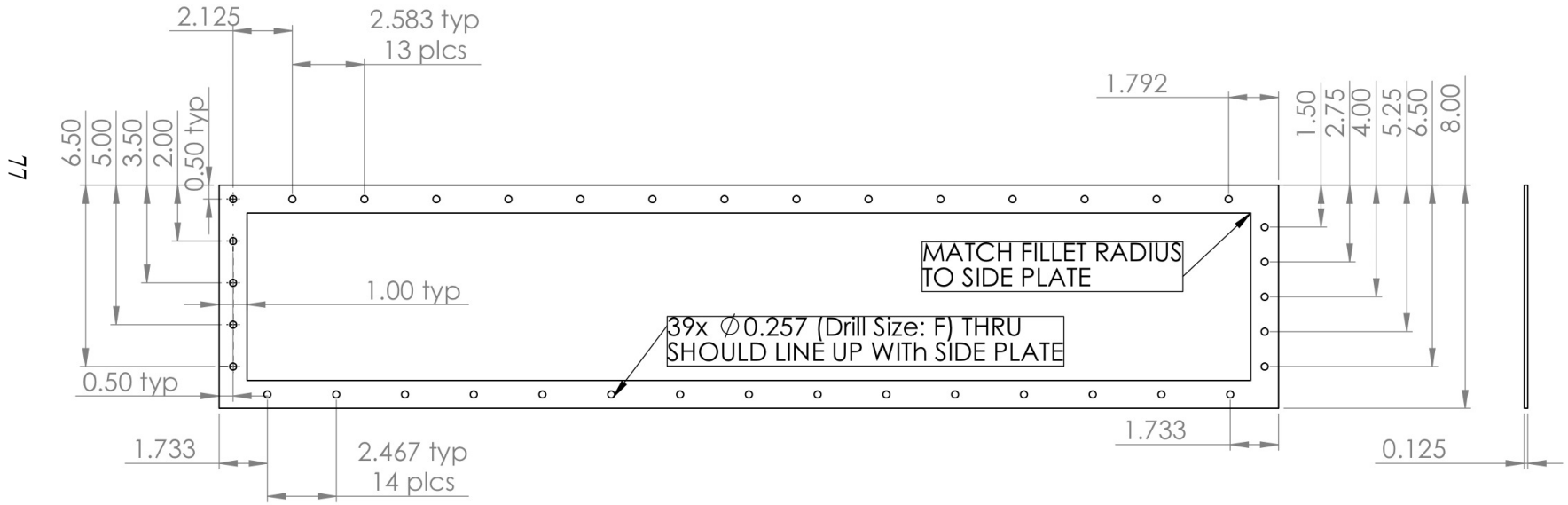

77

DECIMAL POINT	TOLERANCE
0.1	±0.08
0.01	±0.04
0.001	±0.005
UNLESS OTHERWISE SPECIFIED	

Rev. No. 01	Date:06/07/14
Details: Updated holes, width, fillet radius	

PART NAME	SCALE	MATERIAL	QTY	REV
SIDE COVER PLATE	1:5	ALUMINUM	2	-

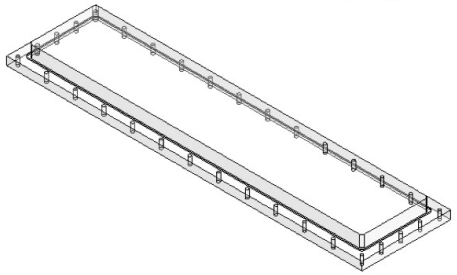

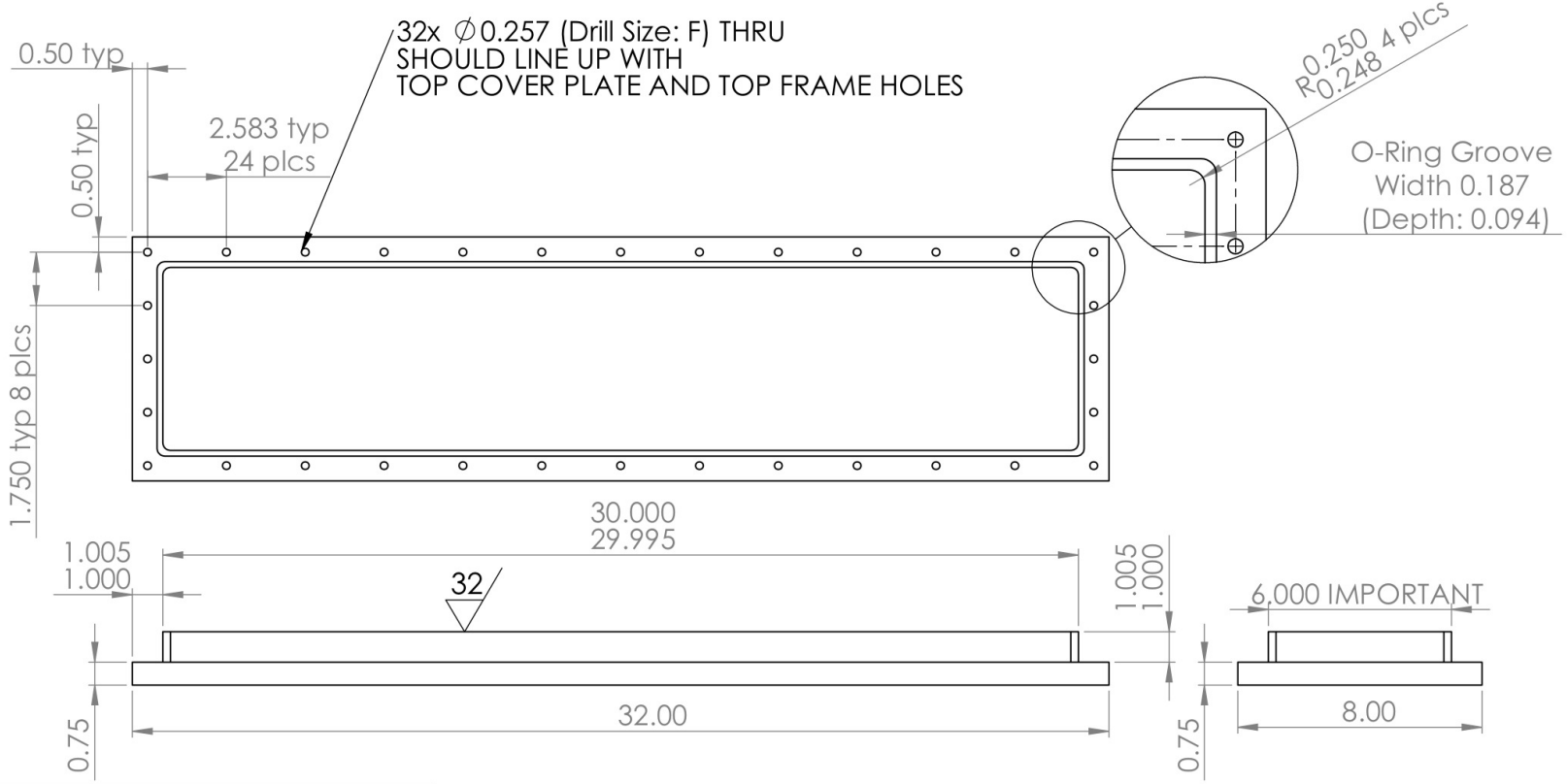

DECIMAL POINT	TOLERANCE
0.1	±0.08
0.01	±0.04
0.001	±0.005
UNLESS OTHERWISE SPECIFIED	

Rev. No. 01	Date: 06/07/14
Details Updated holes, width, O-ring groove, fillet radius	

PART NAME	SCALE	MATERIAL	QTY	REV
TOP PLATE	1:5	ACRYLIC	1	-

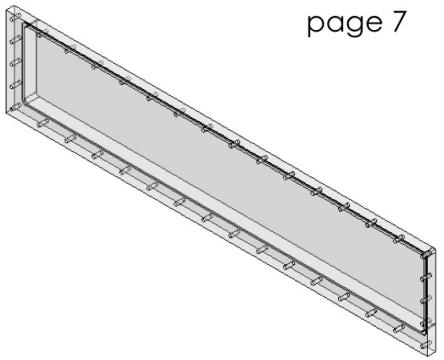

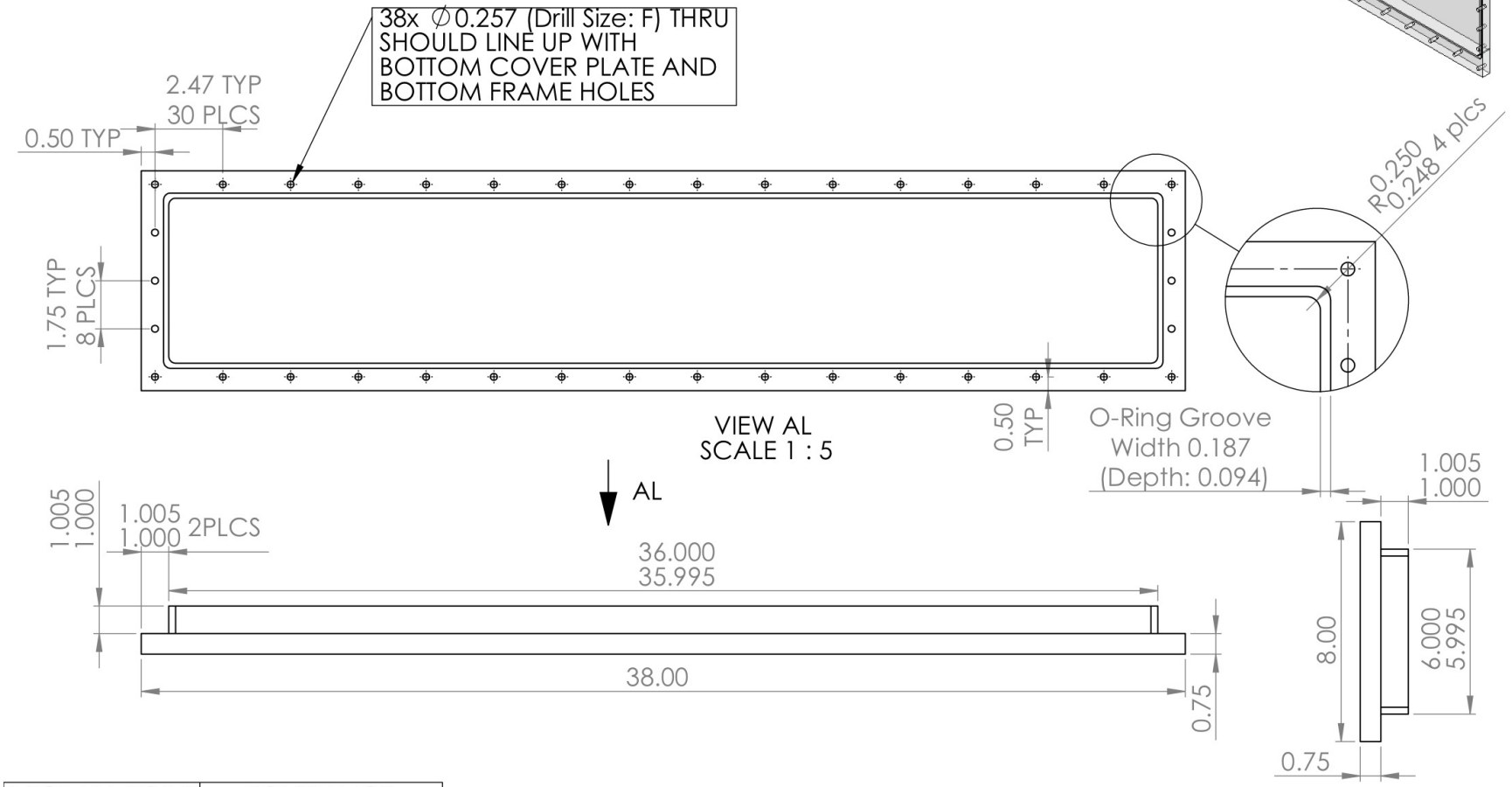

DECIMAL POINT	TOLERANCE
0.1	±0.08
0.01	±0.04
0.001	±0.005
UNLESS OTHERWISE SPECIFIED	

Rev. No. 01	Date: 06/07/14
Details: Updated holes, width, O-ring groove, fillet radius	

PART NAME	SCALE	MATERIAL	QTY	REV
BOTTOM PLATE	1:5	ACRYLIC	1	-

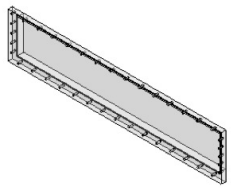

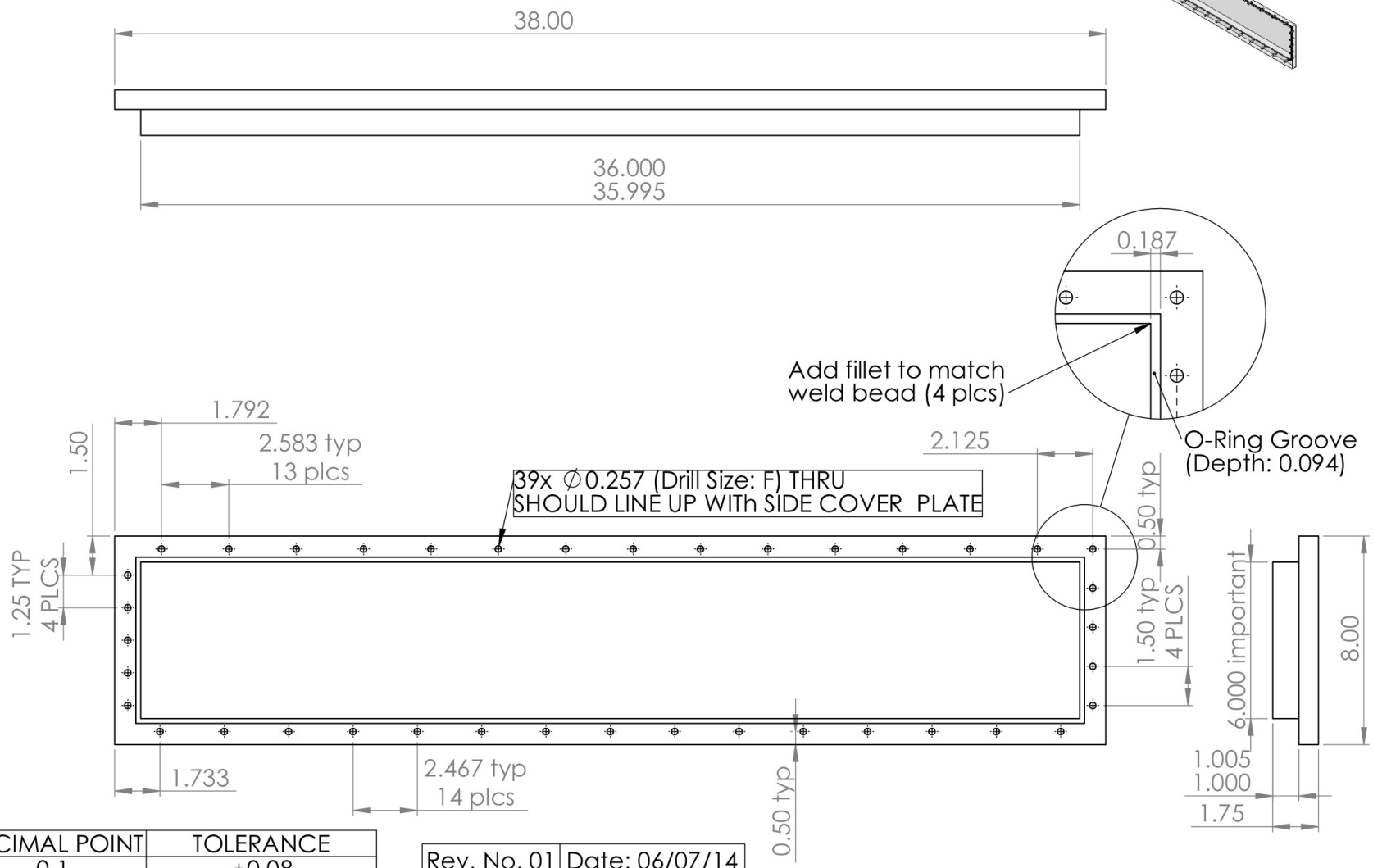

DECIMAL POINT	TOLERANCE
0.1	±0.08
0.01	±0.04
0.001	±0.005
UNLESS OTHERWISE SPECIFIED	

Rev. No. 01	Date: 06/07/14
Details: Updated holes, width, O-ring groove, fillet radius	

PART NAME	SCALE	MATERIAL	QTY	REV
SIDE PLATE	1:5	ACRYLIC	2	-

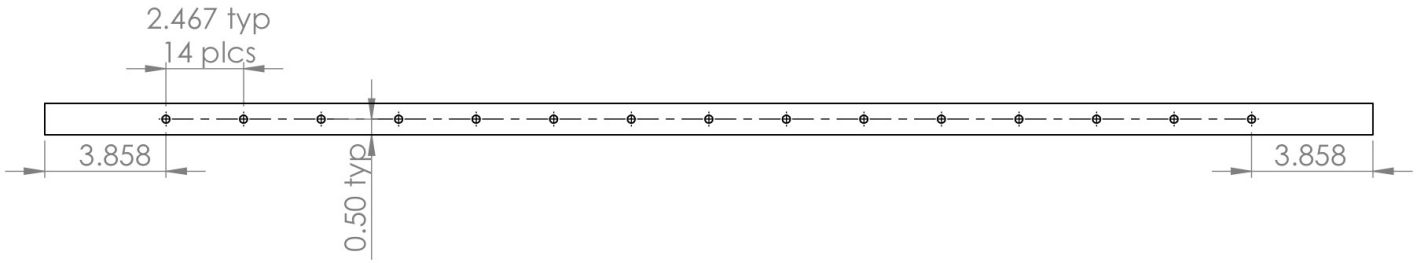

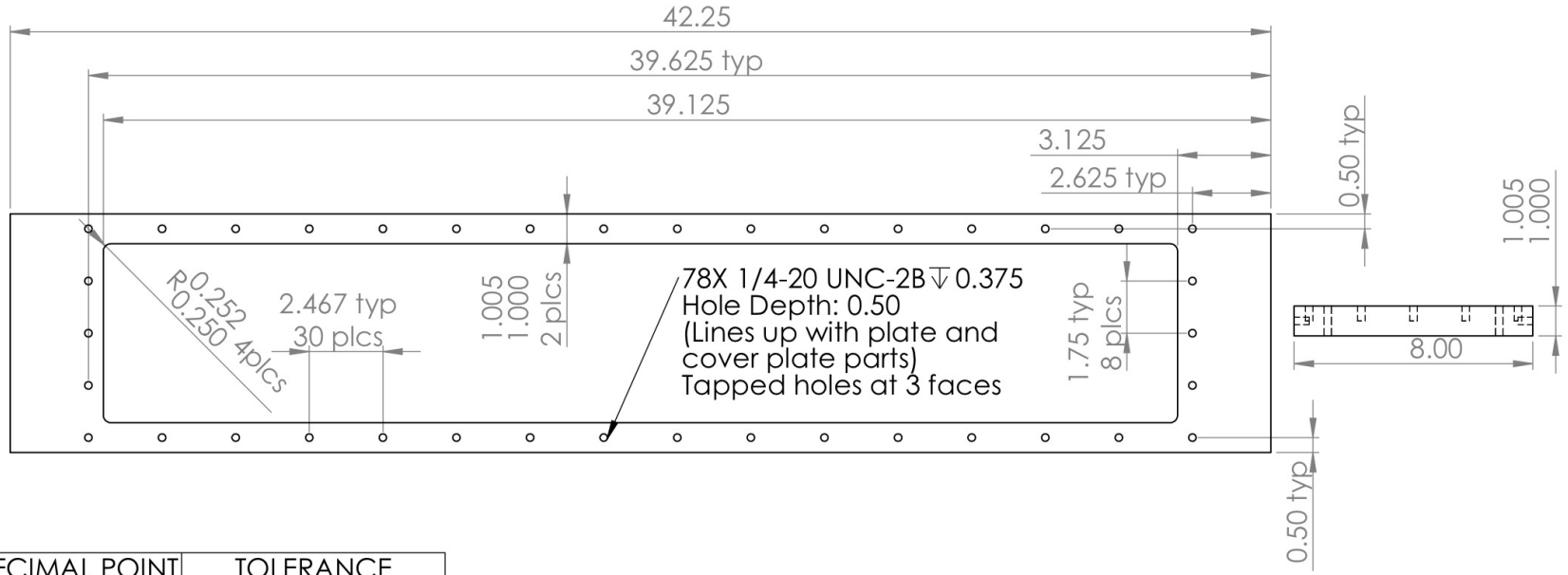

DECIMAL POINT	TOLERANCE
0.1	±0.08
0.01	±0.04
0.001	±0.005
UNLESS OTHERWISE SPECIFIED	

Rev. No. 01	Date: 06/07/14
Details: Updated holes, width, O-ring groove, fillet radius	

PART NAME	SCALE	MATERIAL	QTY	REV
BOTTOM FRAME	1:5	STAINLESS STEEL	1	-

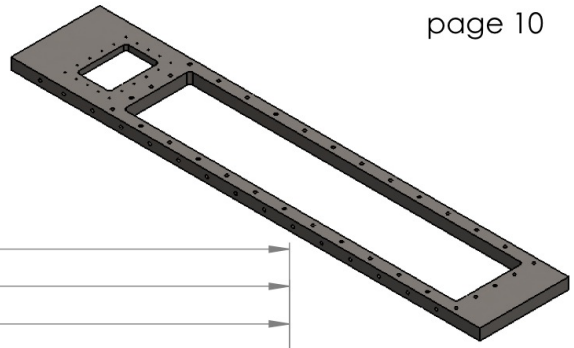

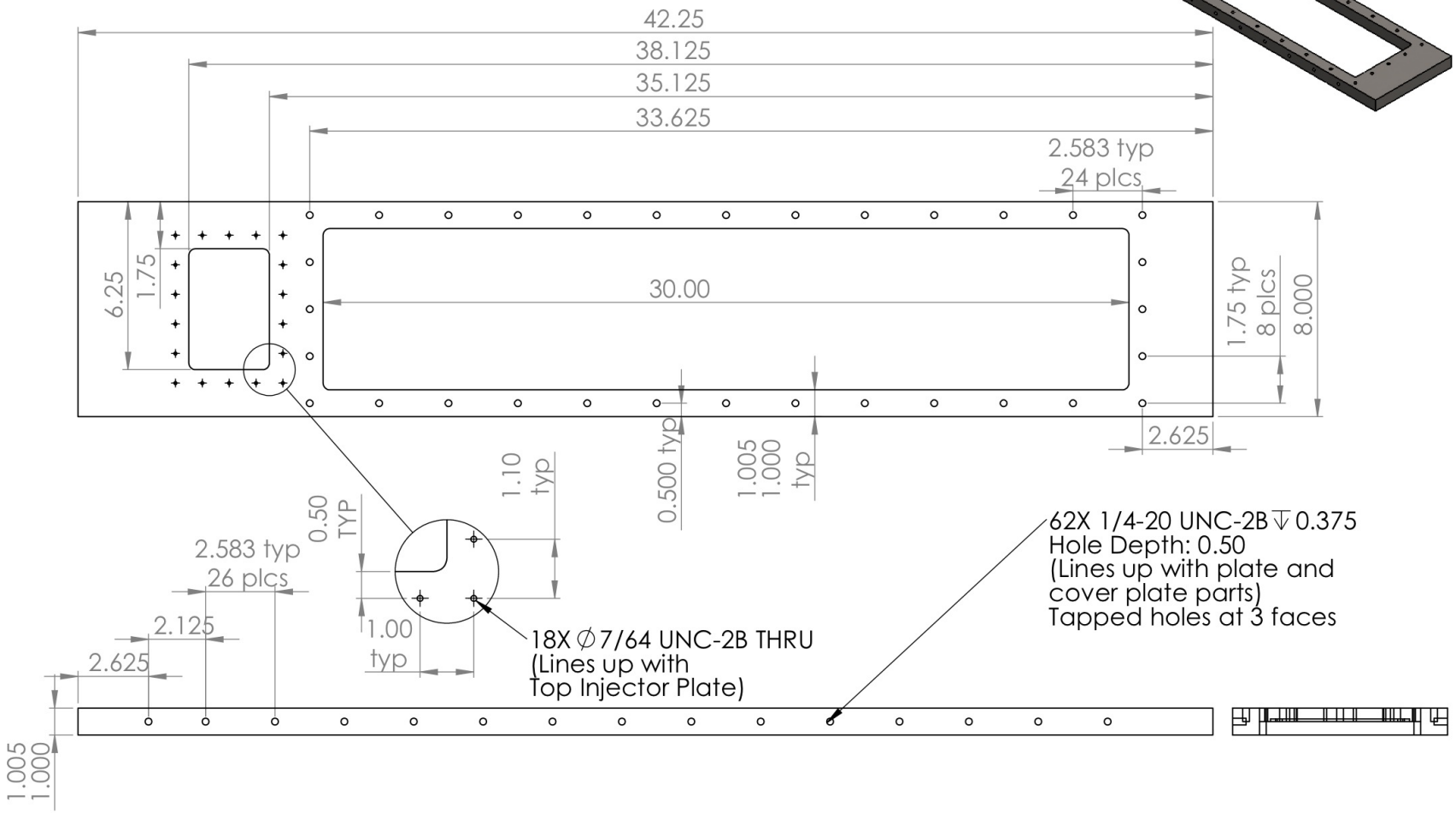

DECIMAL POINT	TOLERANCE
0.1	±0.08
0.01	±0.04
0.001	±0.005
UNLESS OTHERWISE SPECIFIED	

Rev. No. 01	Date: 06/07/14
Details: Updated holes, width, O-ring groove, fillet radius	

See Next Page for 2nd drawing

PART NAME	SCALE	MATERIAL	QTY	REV
TOP FRAME	1:5	STAINLESS STEEL	1	-

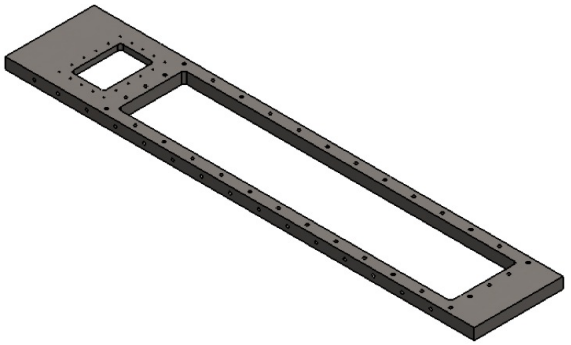

DECIMAL POINT	TOLERANCE
0.1	±0.08
0.01	±0.04
0.001	±0.005
UNLESS OTHERWISE SPECIFIED	

Rev. No. 01	Date: 06/07/14
Details: Updated holes, width, O-ring groove, fillet radius	

PART NAME	SCALE	MATERIAL	QTY	REV
TOP FRAME	1:5	STAINLESS STEEL	1	-

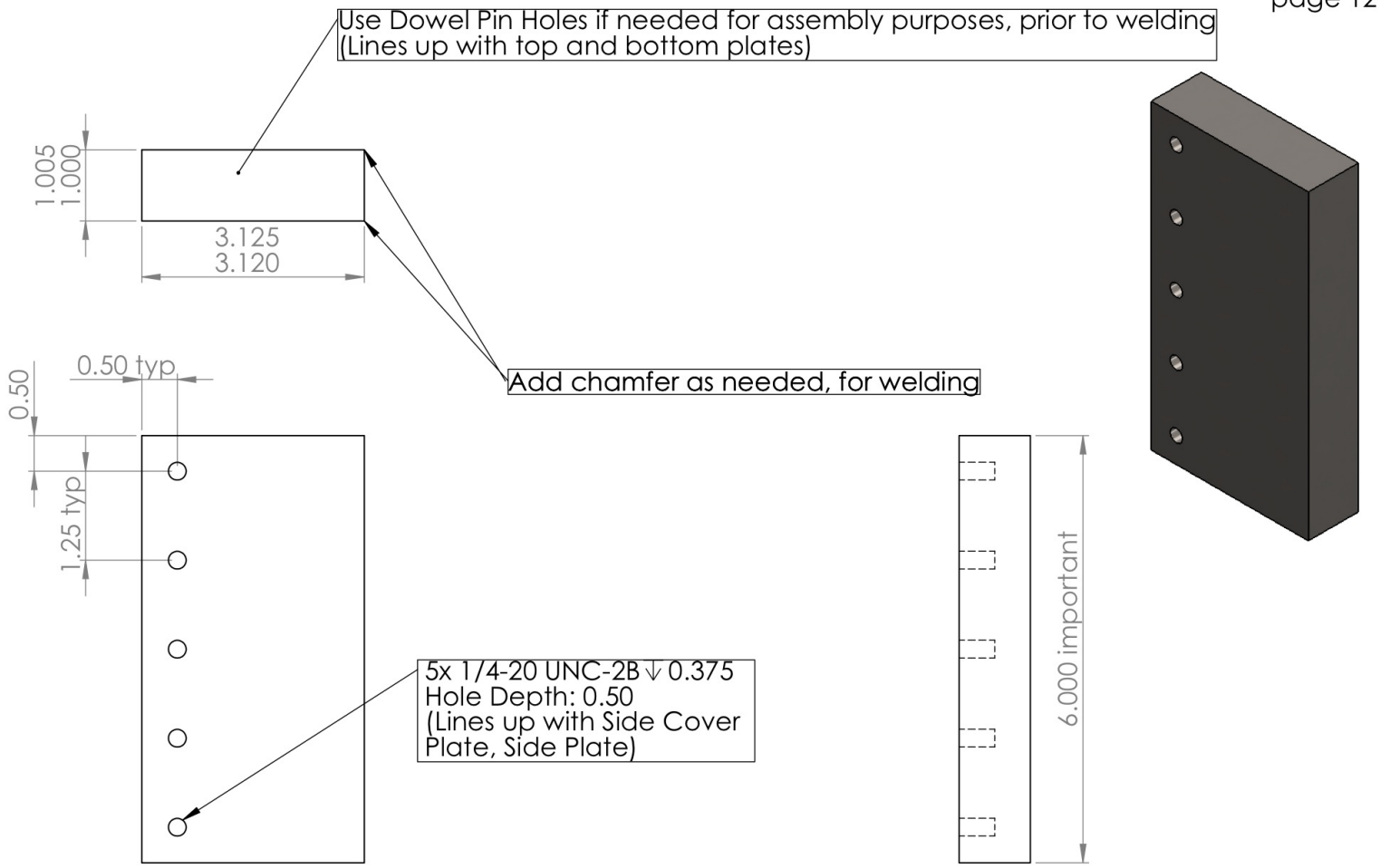

DECIMAL POINT	TOLERANCE
0.1	±0.08
0.01	±0.04
0.001	±0.005
UNLESS OTHERWISE SPECIFIED	

Rev. No. 01	Date: 06/07/14
Details:Updated holes, width, fillet radius	

PART NAME	SCALE	MATERIAL	QTY	REV
SPREADER 4	1:2	STAINLESS STEEL	1	-

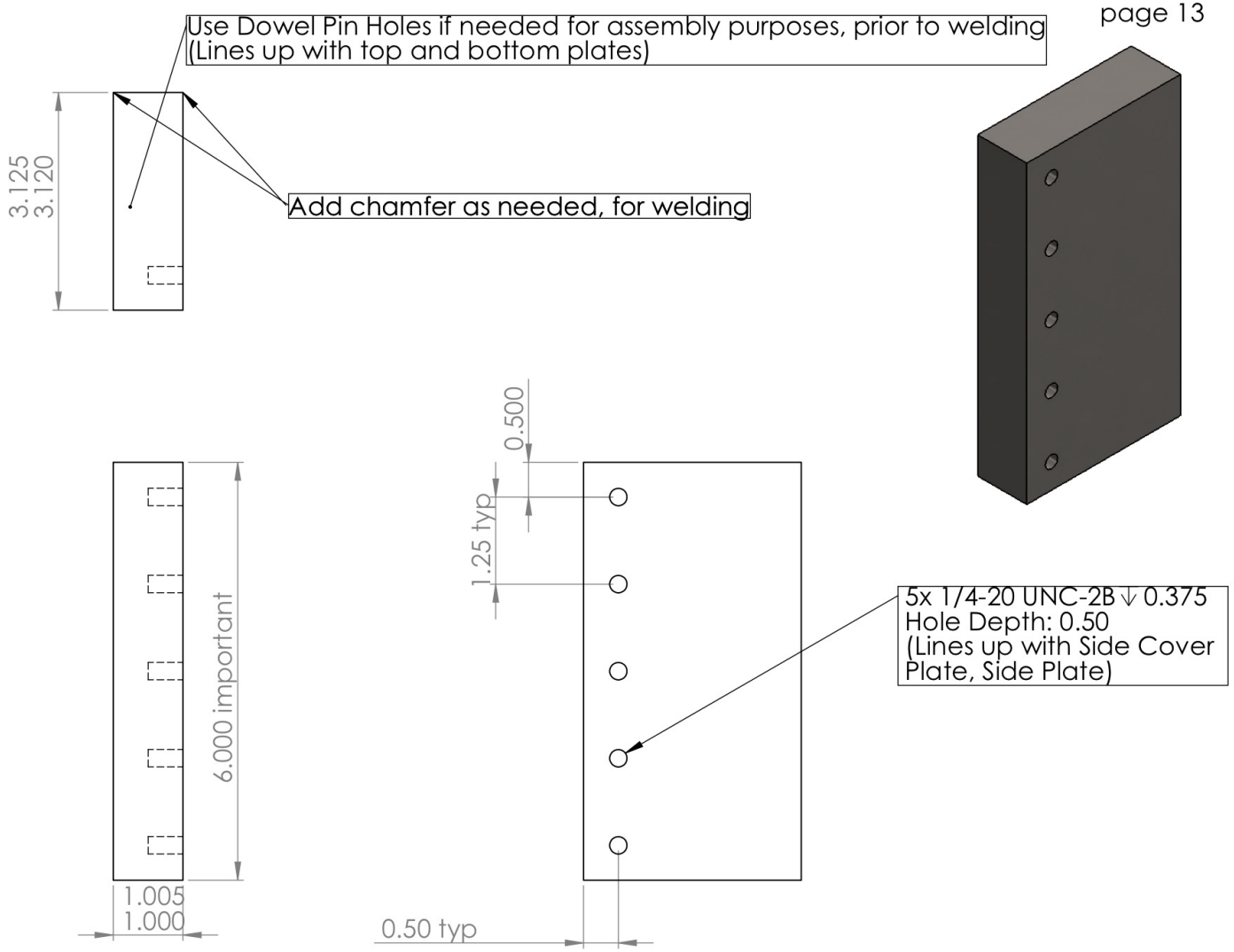

DECIMAL POINT	TOLERANCE
0.1	±0.08
0.01	±0.04
0.001	±0.005
UNLESS OTHERWISE SPECIFIED	

Rev. No. 01	Date: 06/07/14
Details:Updated holes, width, fillet radius	

PART NAME	SCALE	MATERIAL	QTY	REV
SPREADER 3	1:2	STAINLESS STEEL	1	-

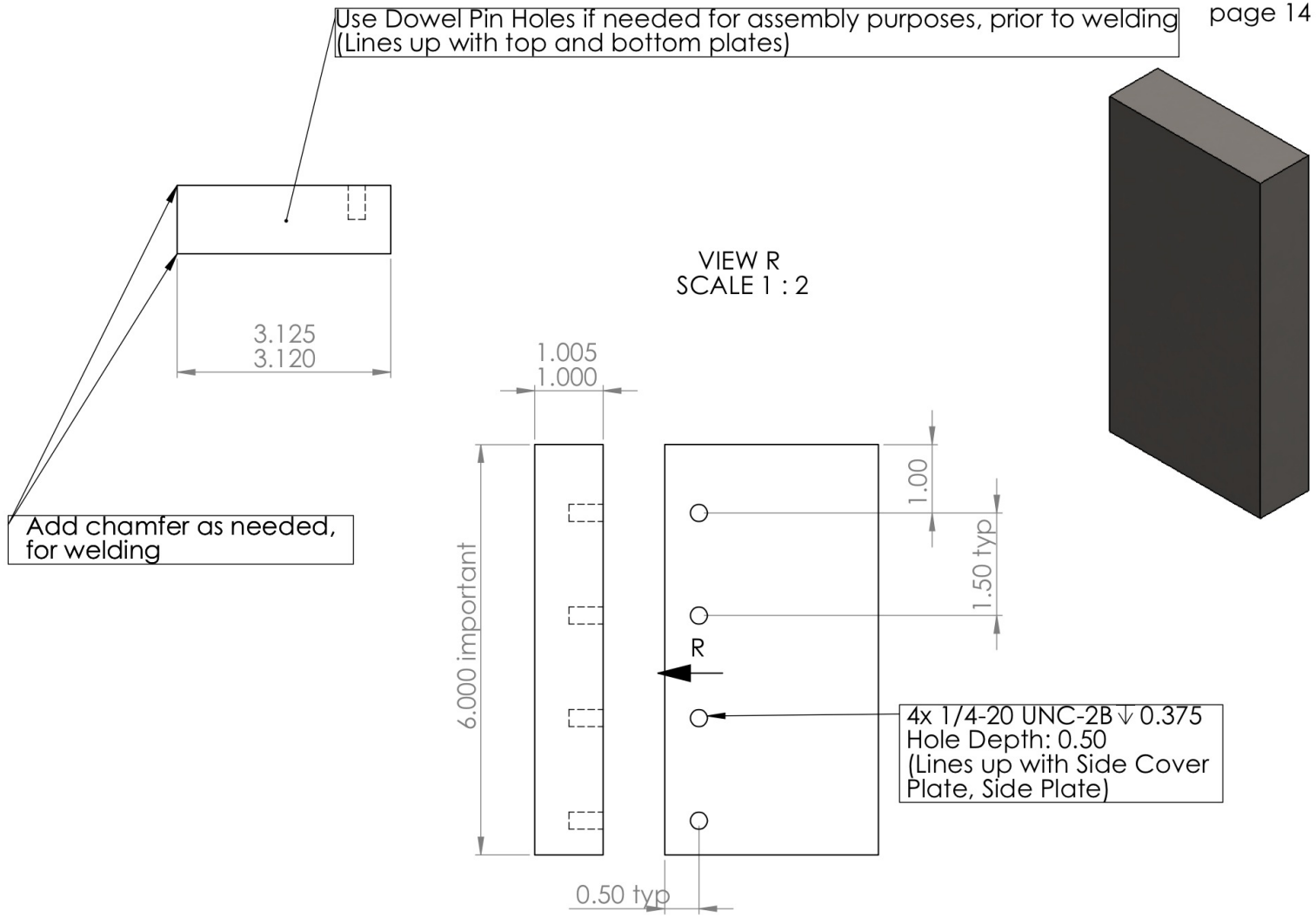

DECIMAL POINT	TOLERANCE
0.1	±0.08
0.01	±0.04
0.001	±0.005
UNLESS OTHERWISE SPECIFIED	

Rev. No. 01	Date: 06/07/14
Details: Updated holes, width, fillet radius	

PART NAME	SCALE	MATERIAL	QTY	REV
SPREADER 2	1:2	STAINLESS STEEL	1	-

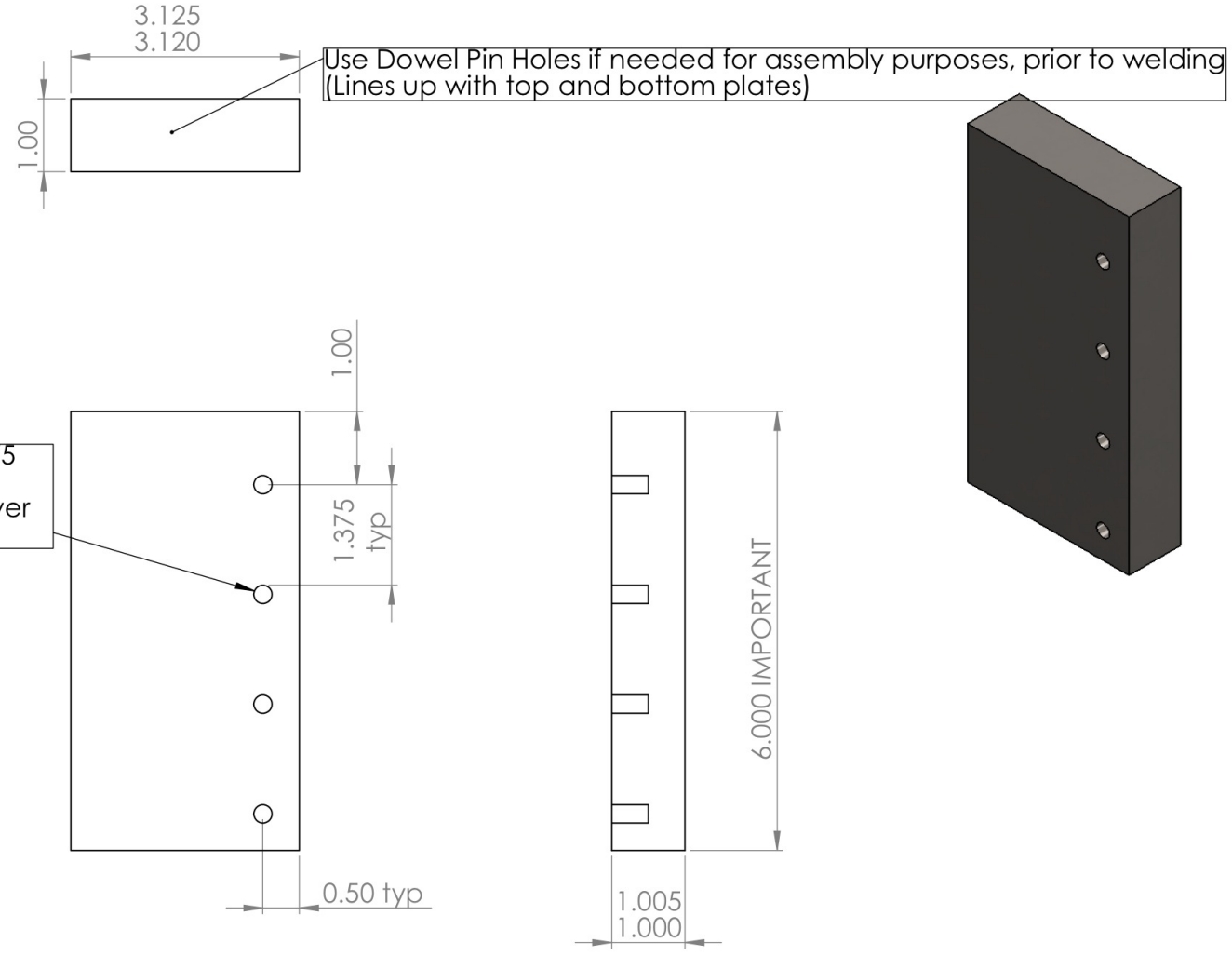

DECIMAL POINT	TOLERANCE
0.1	±0.08
0.01	±0.04
0.001	±0.005
UNLESS OTHERWISE SPECIFIED	

Rev. No. 01	Date:06/07/14
Details:Updated holes, width, fillet radius	

PART NAME	SCALE	MATERIAL	QTY	REV
SPREADER 1	1:2	STAINLESS STEEL	1	-

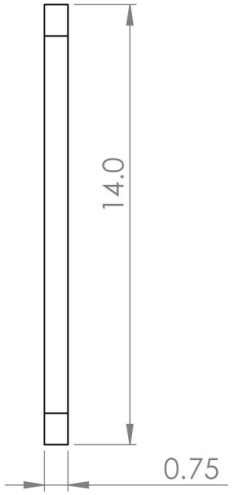

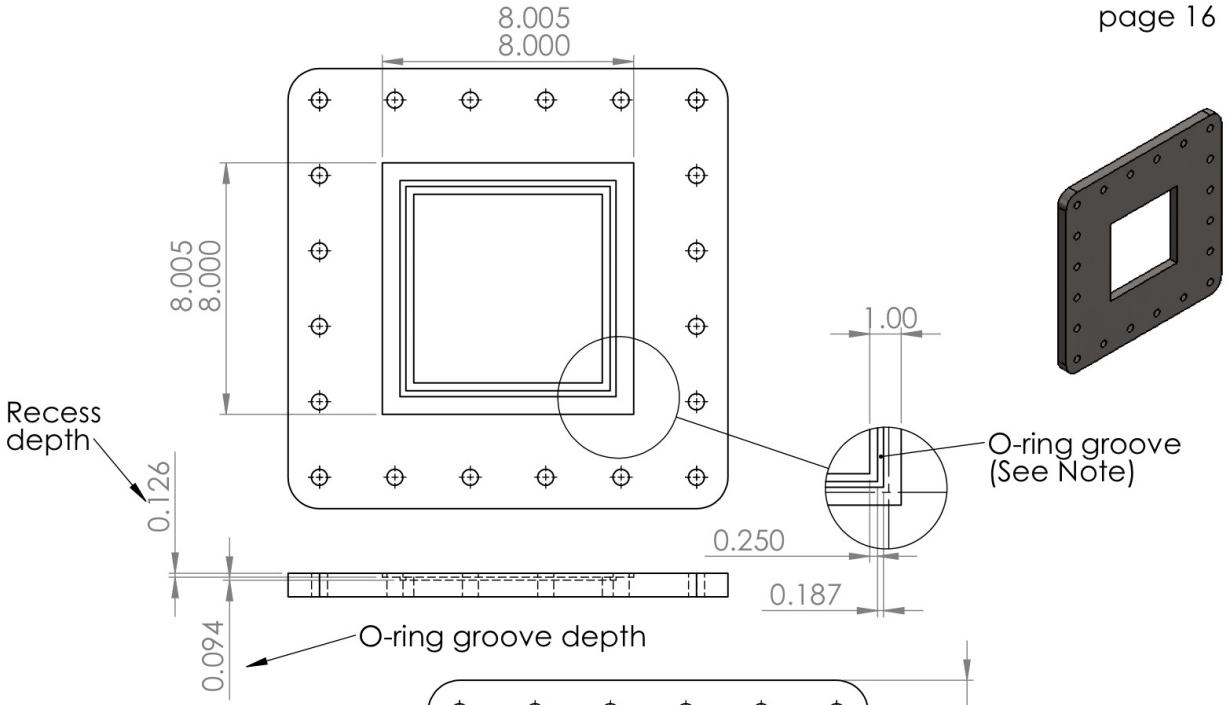

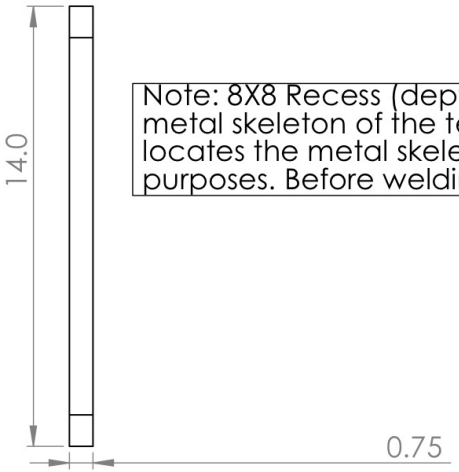

Note: 8X8 Recess (depth: 0.125) fits the metal skeleton of the test section. This locates the metal skeleton for welding purposes. Before welding, install O-ring

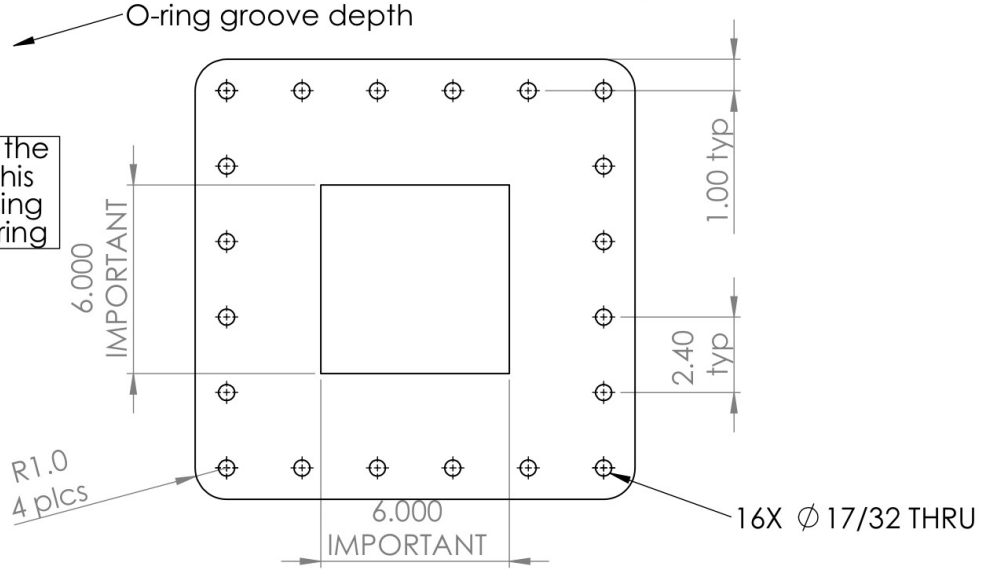

DECIMAL POINT	TOLERANCE
0.1	±0.08
0.01	±0.04
0.001	±0.005
UNLESS OTHERWISE SPECIFIED	

Rev. No. 01	Date: 06/07/14
Details: Updated O-ring groove	

PART NAME	SCALE	MATERIAL	QTY	REV
FLANGES	1:5	STAINLESS STEEL	2	-

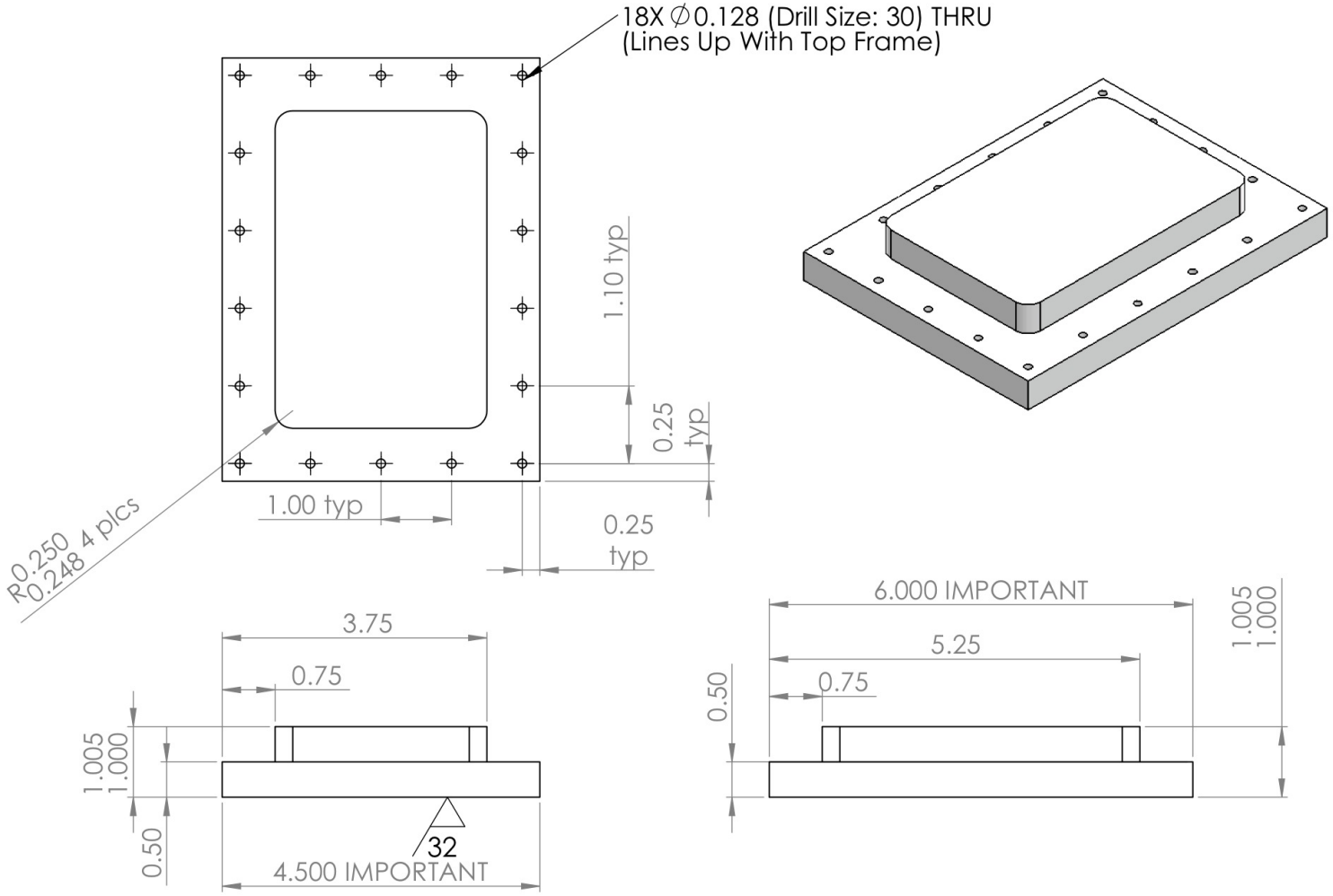

DECIMAL POINT	TOLERANCE
0.1	±0.08
0.01	±0.04
0.001	±0.005
UNLESS OTHERWISE SPECIFIED	

Rev. No. 01	Date:06/07/14
Details:Added fillets	

PART NAME	SCALE	MATERIAL	QTY	REV
TOP INJECTOR PLATE	1:2	ACRYLIC	1	-

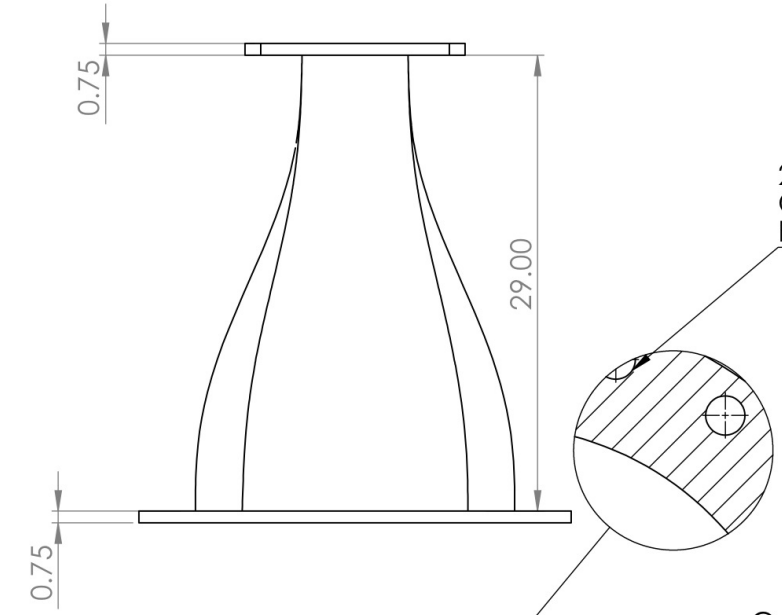

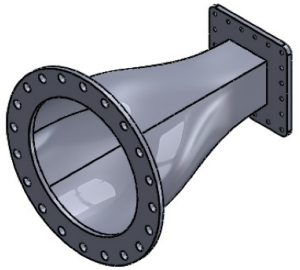

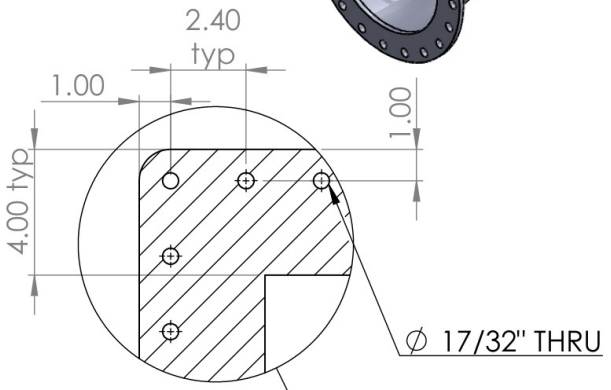

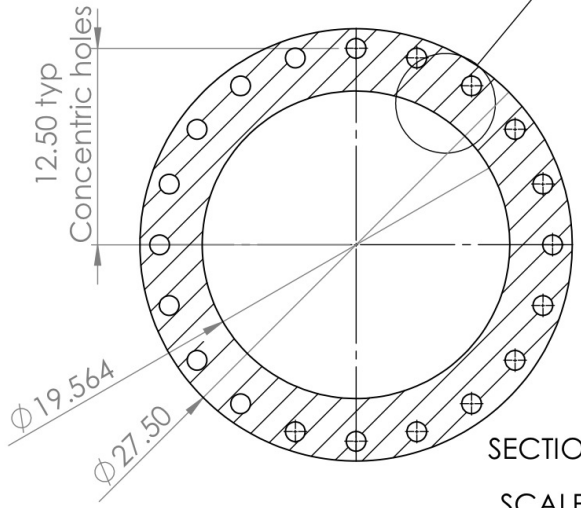

SECTION C-C

SCALE 1 : 10

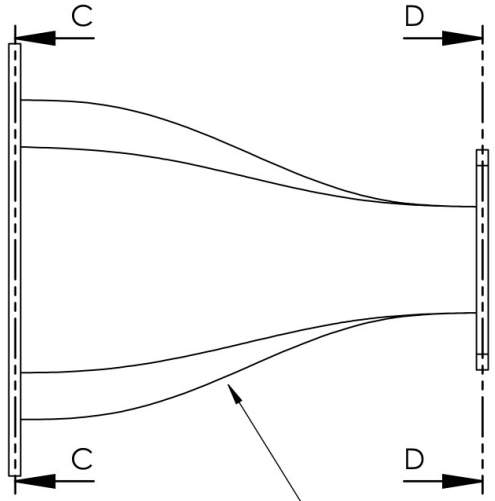

5TH ORDER POLYNOMIAL CURVE

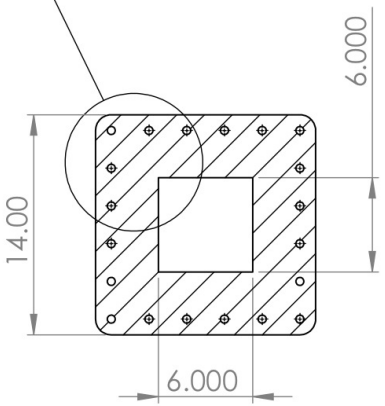

SECTION D-D

SCALE 1 : 10

DECIMAL POINT	TOLERANCE
0.1	±0.08
0.01	±0.04
0.001	±0.005
UNLESS OTHERWISE SPECIFIED	

Rev. No. 3	Date:5/19/14
Details: Change Diameter to 19.564"	

PART NAME	SCALE	MATERIAL	QTY	REV
CONTRACTION	1:10	FIBERGLASS	1	1

06

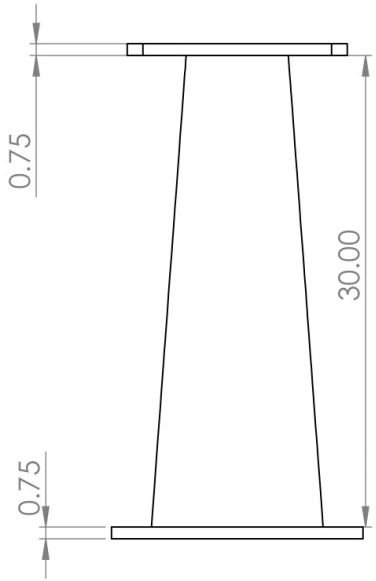

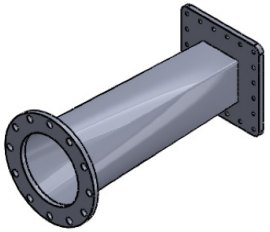

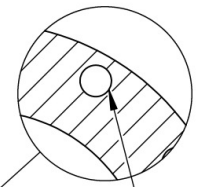

DETAIL G
SCALE 1 : 5

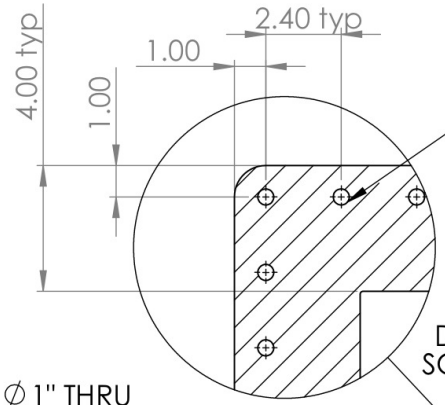

DETAIL H
SCALE 1 : 5

12X ∅1" THRU
Circular Pattern
Fits ANSI Flange

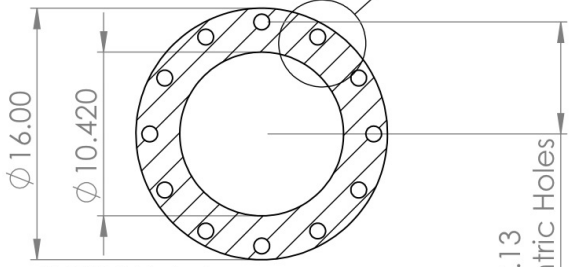

SECTION A-A
SCALE 1 : 10

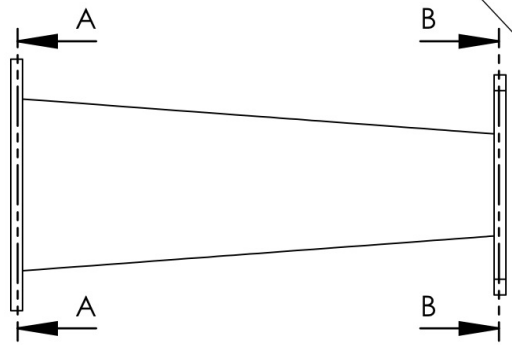

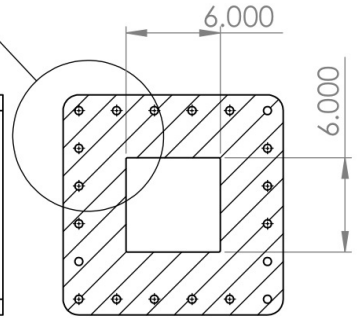

SECTION B-B

SCALE 1 : 10

DECIMAL POINT	TOLERANCE
0.1	±0.08
0.01	±0.04
0.001	±0.005
UNLESS OTHERWISE SPECIFIED	

Rev. No.2	Date: 05/19/14
Details: Change Dimater to 10.42"	

PART NAME	SCALE	MATERIAL	QTY	REV
DIFFUSER	1:10	FIBERGLASS	1	1

VITA

Libin Daniel

Candidate for the Degree of

Master of Science

Thesis: DESIGN AND INSTALLATION OF A HIGH REYNOLDS NUMBER RECIRCULATING WATER TUNNEL

Major Field: Mechanical and Aerospace Engineering

Biographical: Born in Thenmala, Kerala, India on February 10, 1990

Education:

Completed the requirements for the Master of Science in Mechanical and Aerospace Engineering at Oklahoma State University, Stillwater, Oklahoma in July 2014.

Completed the requirements for the Bachelor of Science in Aerospace Engineering at Embry-Riddle Aeronautical University, Prescott, Arizona in December 2012

Experience:

Research and Teaching Assistant, Oklahoma State University, Stillwater, OK
January 2013 – July 2014
Accomplishments:

- Helped in design of a High Reynolds Number Water Tunnel
- Helped in design and setup of experimental fluid dynamics lab courses
- Conducted wind tunnel testing to validate the performance of sUAS
- Helped in calibration of a truck dynamometer
- Graded homework and exams, and held office hours for four courses

Research Assistant, Embry-Riddle Aeronautical University, Prescott, AZ
May 2010- December 2012
Accomplishments:

- Designed and conducted three experimental aerodynamics projects
- Published 'Effect of aspect ratio on gurney-flap Performance' in AIAA Journal of Aircraft
- Published a technical note on the effectiveness of wing root gap as a stall control device

Professional Memberships:

American Institute of Aeronautics and Astronautics (since 2008)
Sigma Gamma Tau (since 2010)
Tau Beta Pi (Delta) (since 2011)